THE RUN-UP AND BACK-WASH PROCESSES OF SINGLE AND DOUBLE SOLITARY WAVES

A Thesis

Presented to the Faculty of the Graduate School

of Cornell University

in Partial Fulfillment of the Requirements for the Degree of

Master of Science

by

Hong Yueh Lo

January 2013

ABSTRACT

The run-up and back-wash processes of single and double solitary waves on a slope were studied experimentally. Experiments were conducted in three different wave flumes with four different slopes. For single solitary wave, new experimental data were acquired and, based on the theoretical breaking criterion, a new surf parameter specifically for breaking solitary waves was proposed. An equation to estimate maximum fractional run-up height on a given slope was also proposed. For double solitary waves, new experiments were performed by using two successive solitary waves with equal wave heights; these waves were separated by various durations. The run-up heights of the second wave were found to vary with respect to the separation time. Particle image velocimetry measurements revealed that the intensity of the back-wash flow generated by the first wave strongly affected the run-up height of the second wave. Showing trends similar to that of the second wave run-up heights, both the back-wash breaking process of the first wave and the reflected waves were strongly affected by the wave-wave interaction. Empirical run-up formula for the second solitary wave was also introduced.

BIOGRAPHICAL SKETCH

Lo grew up in Taipei City, Taiwan, and pursued post-secondary education in the U.S. He attended Green River Community College in Washington State for two years before transferring to Cornell University as a junior, and in 2011 received a Bachelor of Science in Civil and Environmental Engineering. Enrolled in the M.S./Ph.D. program in the same department, he furthers his graduate study at Cornell University. An outdoor enthusiast, Lo is especially fascinated by fluids in the environment, be it the ocean, lakes, rivers, or snow. It is this passion that drives him to research environmental fluid mechanics.

I love you, Mom, Dad, and Sister.

ACKNOWLEDGEMENTS

I was fortunate to have become part of the research group before Dr. Yong Sung Park left. His first-hand experience with laboratory work and practical inputs have greatly enhanced my ability to conduct experiments and data analysis. I would not have been able to progress efficiently without my advisor Philip L.-F. Liu's insightful ideas and suggestions. Lastly, I am grateful to my family and Dr. Chien-Hsiung Yang for their support.

TABLE OF CONTENTS

LIST OF TABLES

LIST OF FIGURES

CHAPTER 1

INTRODUCTION

1.1 Literature review

Solitary waves have been commonly used to model long water waves, in part due to the easiness to realize them in the laboratory. The run-up of single solitary waves on a slope has been extensively investigated. For example, *Hall and Watts* [1953] carried out run-up height measurements with various wave-height-to-water-depth ratios on five different slopes. *Synolakis* [1987] derived analytical solutions describing the evolution and run-up process of a non-breaking solitary wave on a uniform slope, and validated them with experiments on a 1/19.85 slope. The theory will be briefly reviewed in Section 1.3. Experiments on breaking solitary waves on the same slope were also conducted in *Synolakis*' study. More recently, *Hsiao et al.* [2008] and *Chang et al.* [2009] investigated solitary wave run-up in a large-scale wave tank on 1/60 and 1/20 slopes, respectively. Other reported experimental data include: *Langsholt* [1981], *Gjevik and Pedersen* [1981], *Zelt* [1991], *Briggs et al.* [1995], *Li and Raichlen* [2001] [2002], and *Jensen et al.* [2003]. Various empirical formulas for maximum run-up heights of breaking solitary wave have been proposed with different range of applicability.

Numerically, *Zelt* [1991] developed a finite element model for solving the Boussinesq equations and calculated run-up heights on various slopes and proposed an artificial bottom-friction factor to monitor run-up heights on different slopes. Solving the fully non-linear free-surface potential flow problem with an integral equation method, *Grilli et al.* [1997] classified solitary wave breaking

based on numerical simulations. On the other hand, *Li and Raichlen* [2002] computed run-up heights for both breaking and non-breaking solitary waves using a shock capturing model. *Kobayashi and Karjadi* [1994] and *Fuhrman and Madsen* [2008] explored the possibility of introducing a surf parameter to characterize the run-up of breaking solitary waves.

Compared to the rich literature on single solitary wave run-up, little information on the run-up process of multiple solitary waves is available, which can have important application on estimating the run-up of waves with multiple crests. Undular bores have been observed during tsunami events (e.g., *Grue et al.* [2008], *Madsen et al.* [2008], and Figure 1.1) and can be viewed as combination of solitary waves with different wave heights and different separation times among them. *Peregrine* [1966] pointed out that undular bores tend to grow into a succession of solitary waves, while recently *El et al.* [2012] showed by theory that a sequence of isolated leading solitons forms as an undular bore propagates into decreasing water depth, although the relevant geophysical scale has not been explicitly discussed. Thus, there is a need to perform controlled experiments so as to gain a better understanding of the run-up process associated with multiple solitary waves.

To make the problem more tractable, as a first step we seek to experimentally study two identical solitary waves separated by various separation times. We remark that *Raichlen* (unpublished data, 1985) is the first to perform run-up measurements on double solitary waves, with limited wave conditions on two different slopes. In this study, we examine the run-up and back-wash processes in-depth, with a wide range of wave conditions on different slopes to investigate the observed run-up trend, and extend current knowledge in single solitary

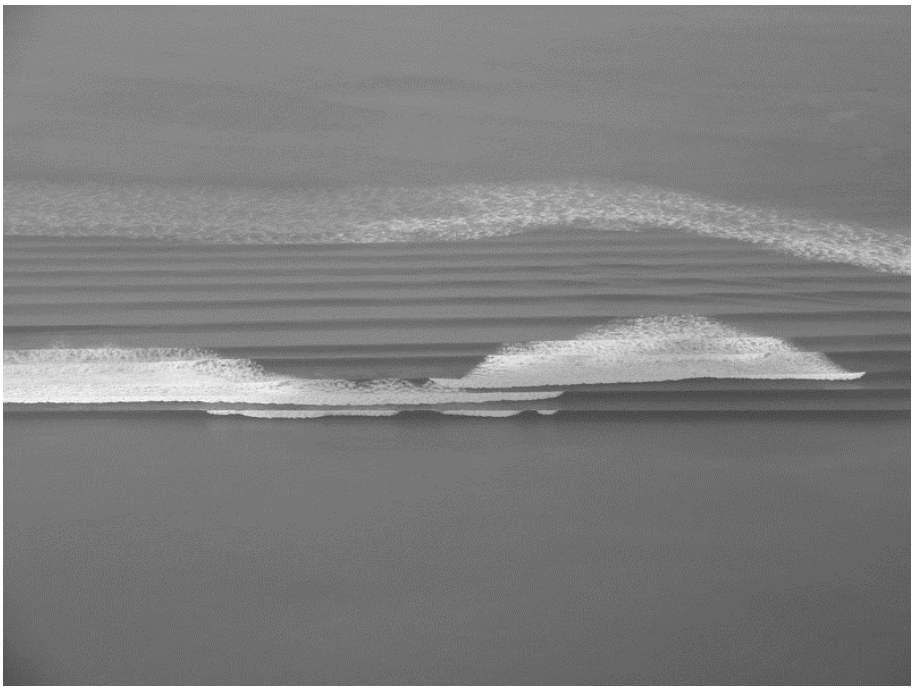

Figure 1.1: The 2004 Sumatra tsunami observed on Koh Jum island, Thailand, shows the characteristics of an undular bore (copyright Anders Grawin).

wave to the double solitary waves scenario.

Additional experiments for single solitary wave run-up are performed not only to enrich the data base, but also to serve as references for the double solitary wave experiments. In re-analyzing existing run-up data for single solitary waves, we define a new surf parameter for solitary wave, based on the wave breaking criterion following *Carrier and Greenspan*'s [1958] theory. The new surf parameter has a slightly different form from those suggested by *Kobayashi and Karjadi* [1994] and *Fuhrman and Madsen* [2008], but it is theoretically grounded.

In the next section, we shall introduce relevant physical and dimensionless parameters to be used in this study, and then briefly review the theoretical work on the run-up of solitary waves. We will then describe the laboratory setups

and experimental methods, followed by the presentation of results. The run-up heights of single solitary waves will be discussed first. Special attention shall be paid to the definition of the surf parameter characterizing wave breaking and run-ups. The approach in analyzing single solitary waves is extended to double solitary waves. Empirical formulae for the run-up height ratio of two solitary waves are computed. The back-wash breaking, particle image velocimetry (PIV) measurements, and the reflected waves will then be examined accordingly and their relevance explained.

1.2 Definitions and parameters

In studying the run-up of single and double solitary waves the following physical parameters are involved: h is the constant water depth up to the toe of the slope; s is the slope expressed in terms of vertical rise divided by horizontal run; η is the surface elevation from the still water level; H is the solitary wave height in the constant depth region; τ is the separation time between the two solitary wave peaks; and R is the vertical run-up height caused by the waves (R_1 and R_2 represent the run-up heights of the first and the second wave, respectively, when double solitary wave is considered). With the above definitions, relevant normalized parameters include: wave height H/h, separation time τ/T where T is the effective wave period to be defined, run-up R/h or R/H, and relative run-up R_2/R_1. The setup and parameters are illustrated in Figure 1.2.

For a solitary wave travelling at speed c in the ξ-direction, the leading-order solution in constant depth is well-known:

$$\eta(\xi,t) = H\mathrm{sech}^2[K(\xi - ct)], \quad \text{where} \quad K = \frac{1}{h}\sqrt{\frac{3H}{4h}}, \quad \text{and} \quad c = \sqrt{g(H+h)}, \quad (1.1)$$

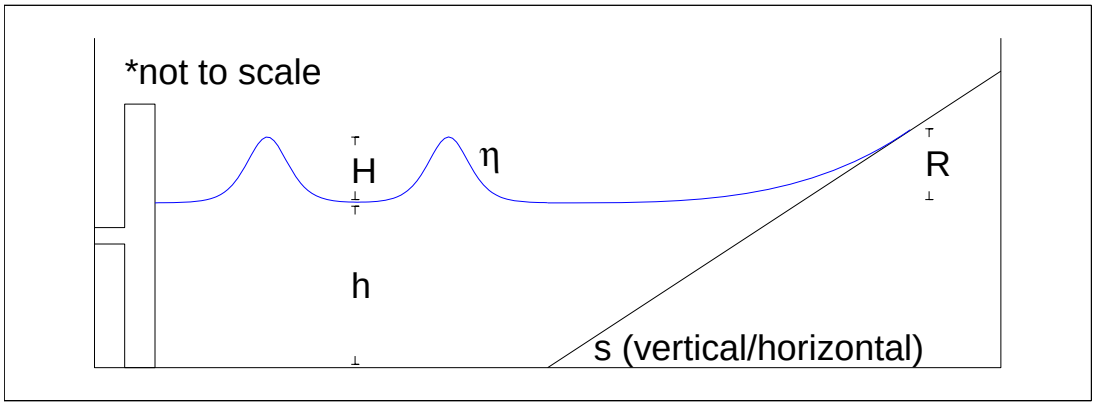

Figure 1.2: Illustration of the setup and some relevant parameters.

and

$$\lambda = \frac{2\pi}{K}, \quad \text{and} \quad T = \frac{2\pi}{Kc}, \tag{1.2}$$

can be viewed as the effective wavelength and effective wave period, respectively. While $2H/\lambda$ measures the steepness of the solitary wave front, $l = \lambda/2$ characterizes the effective length of the wave front. Since $L = h/s$ is the horizontal length of the beach slope, another relevant dimensionless parameter is the horizontal length ratio, l/L. In the case of a solitary wave, l/L can be expressed as

$$\frac{l}{L} = \frac{\lambda}{2L} = \left(\frac{2\pi}{\sqrt{3}}\right)(s)\left(\frac{H}{h}\right)^{-\frac{1}{2}}. \tag{1.3}$$

1.3 Review of Solitary Wave Run-up Theory

In this section we will review the theoretical derivation shown by *Synolakis* [1987], where *Carrier and Greenspan*'s [1958] transformation was used to solve the non-linear shallow water equations applied to solitary waves travelling from constant depth onto a plane slope. The setup is similar to that shown in Figure (1.2).

To begin with, the dimensionless parameters (for use in this section only) are introduced as follows: u is the depth-average horizontal velocity normalized by $\sqrt{gh}$, d the local water depth normalized by h, ζ the free surface elevation normalized by h, x the horizontal spatial coordinate normalized by h, and t the temporal coordinate normalized by $\sqrt{g/h}$. $x = 0$ at the initial shoreline and $x > 0$ offshore. Since we have a constant depth region attached to a plane slope, the variable local water depth

$$\begin{cases} d(x) = xs, \quad for \quad x \le \frac{1}{s} \\ d(x) = 1, \quad for \quad x > \frac{1}{s} \end{cases}. \tag{1.4}$$

With the above dimensionless variables, the non-dimensional non-linear shallow water equations can be written as

$$\begin{cases} h_t + (hu)_x = 0 \\ u_t + uu_x + u_x = 0 \end{cases}, \tag{1.5}$$

where the subscripts indicate the variables with respect to which the derivatives are taken.

To solve (1.5), *Carrier and Greenspan* [1958] proposed the following hodograph transformation:

$$\begin{cases} u = \frac{\psi_\sigma}{\sigma} \\ \zeta = \frac{1}{4}\psi_\beta - \frac{1}{2}u^2 \\ x = \frac{1}{s}(\frac{1}{16}[\sigma^2 - \frac{1}{4}\psi_\beta + \frac{1}{2}u^2]) \\ t = \frac{1}{s}(\frac{\psi_\sigma}{\sigma} - \frac{1}{2}\beta) \end{cases}, \tag{1.6}$$

where $\sigma = 0$ always corresponds to the shoreline.

This transformation allows us to convert (1.5) into a linear equation in the (σ, β) domain:

$$(\sigma\psi_\sigma)_\sigma = \sigma\psi_{\beta\beta} \tag{1.7}$$

If we assume small incident wave height in the constant depth region so that the linear wave composition for solitary waves applies, we can use it to specify the boundary condition at the toe of the slope ($X_0 = 1/s$):

$$\eta(X_0, t) = \int_{-\infty}^{\infty} \phi(k) e^{-ikct} dk, \tag{1.8}$$

where $\phi(k) = \frac{2}{3} kcsch(\pi k/2K) e^{ikX_1}$, K is defined in (1.1), and X_1 is the location of the center of the solitary wave at $t = 0$.

Converting the boundary condition from the (x, t) domain to the (σ, β) domain, however, is not trivial. *Synolakis* suggests that if non-linearity is insignificant, the $O(u^2)$ terms can be neglected in the conversion, so that (1.6) becomes

$$u = \frac{\psi_\sigma}{\sigma}, \zeta = \frac{1}{4}\psi_\beta, x = \frac{1}{16s}\sigma^2, \text{ and } t = -\frac{1}{2s}\beta. \tag{1.9}$$

If the boundary condition is specified as such and the Fourier integral theorem applied repeatedly, *Synolakis* showed that the solution to (1.7) is

$$\psi(\sigma, \beta) = -\frac{16i}{X_0} \int_{-\infty}^{\infty} \frac{\phi(k)}{k} \frac{J_0(\frac{1}{2}\sigma k X_0) exp[-ikX_0(1 - \frac{1}{2}\beta)]}{J_0(2kX_0) - iJ_1(2kX_0)} dk, \tag{1.10}$$

where J is the Bessel function of the first kind.

Based on (1.10) it can then be shown that for solitary waves the run-up (as a function of time)

$$\frac{R(t)}{h} = \frac{4}{3} \int_{-\infty}^{\infty} kcsch(\frac{\pi k}{2K}) \frac{exp[ik(X_1 - X_0 - ct)]}{J_0(2kX_0) - iJ_1(2kX_0)} dk, \tag{1.11}$$

which will be referred to as the run-up integral herein (the maximum value of this function is the maximum run-up). *Synolakis* further showed that, if $(H/h)^{1/2} \gg 0.288s$, (1.11) can be simplified into the run-up law

$$\frac{R}{h} = 2.831(s)^{-\frac{1}{2}} (\frac{H}{h})^{\frac{5}{4}}. \tag{1.12}$$

We note that while easy to use, (1.12) is an asymptotic approximation of (1.11); to accurately evaluate the maximum run-up resulting from *Synolakis'* derivation, the maximum value of (1.11) should be considered.

For the solution (1.10) to be valid, the Jacobian of the transformation (1.6) can never equal to zero, so that the transformation from (x,t) to (σ,β) is always one-to-one, i.e. the free surface never becomes vertical. *Synolakis* showed that this requirement implies

$$\frac{H}{h} < 0.8183 s^{\frac{10}{9}}, \tag{1.13}$$

which can be seen as the theoretical wave breaking criterion, where waves break during run-up if H/h exceeds the threshold value on the right hand side. Similarly, *Madsen and Schäffer* [2010] derived the breaking criterion during back-wash - waves break during back-wash if

$$\frac{H}{h} > 0.5139 s^{\frac{10}{9}}, \tag{1.14}$$

CHAPTER 2

EXPERIMENTS

2.1 Wave flumes

Experiments were performed in three wave flumes with four different beach slopes. The three facilities include two medium-sized wave flumes in the De-Frees Hydraulic Laboratory at Cornell University and the large wave flume in the O. H. Hinsdale Wave Research Laboratory at Oregon State University. In each wave flume a piston-type wave-maker is installed on one end of the flume, and on the other end of the flume is a uniform slope; between the wave-maker and the toe of the slope is a constant depth region. Four different slopes are used in the experiments. Table 2.1 lists the dimensions, materials, and beach slopes of each wave flume. From herein each experiment is identified by the associated beach slope.

To measure water surface displacement, acoustic wave gauges (Banner Engineering S18U) with 0.5 mm manufacturer-specified resolution, were used in the wave flumes at Cornell University; resistance-type wave gauges with estimated

Table 2.1: Flume dimensions and slope materials.

Slope	Length × Width × Height	Flume wall material	Slope material
1 / 2.47	34 m × 0.6 m × 0.9 m	Glass	Glass
1 / 10	12 m × 0.8 m × 1 m	Glass	Glass
1 / 12	104 m × 3.7 m × 4.6 m	Concrete	Concrete
1 / 20	34 m × 0.6 m × 0.9 m	Glass	Glass & styrene

resolution between 1 mm and 1 cm were employed in the large-scale flume at the O. H. Hinsdale Wave Research Laboratory. Video cameras were placed on top of the slopes to measure wave run-up heights. Grids or fiducial marks on the slope allow conversion of pixels in the videos to the known length.

2.2 Wave generation

By using *Goring*'s [1978] method, single and double solitary waves were generated. Figure 2.1 shows a typical wave-maker trajectory for generating a solitary wave (note that the wave-maker's definition of negative displacement is towards the beach slope). *Grimshaw*'s [1971] second-order solitary wave solution is used to check the accuracy of wave shapes. Overall, solitary wave shapes generated in the experiments are highly accurate; see Figure 2.1 for comparisons. The wave conditions of the single solitary waves considered are listed in Table 2.2.

Table 2.2: Experimental wave conditions of single solitary waves. *From *Raichlen* (unpublished data, 1985), which will be shown with present results herein.

Slope	h(m)	H / h	R / h	Back-wash breaking (2.2)	Run-up breaking (2.1)	Run-up breaking (2.3)
1 / 2.47	0.2	0.049	0.097	No	No	No
1 / 2.47	0.2	0.101	0.230	No	No	No
1 / 2.47	0.2	0.149	0.378	No	No	No
1 / 2.47	0.2	0.202	0.533	Yes	No	No

1 / 2.47	0.2	0.250	0.686	Yes	No	No
1 / 2.47	0.2	0.302	0.854	Yes	Yes	No
1 / 2.47	0.15	0.346	0.979	Yes	Yes	No
1 / 2.47	0.15	0.394	1.129	Yes	Yes	No
1 / 2.47	0.15	0.448	1.294	Yes	Yes	No
1 / 2.47	0.15	0.498	1.458	Yes	Yes	No
1 / 2.55*	unknown	0.225	0.593	Yes	No	No
1 / 10	0.5	0.005	0.008	No	No	No
1 / 10	0.5	0.007	0.015	No	No	No
1 / 10	0.5	0.010	0.028	No	No	No
1 / 10	0.5	0.015	0.045	No	No	No
1 / 10	0.5	0.019	0.064	No	No	No
1 / 10	0.5	0.024	0.079	No	No	No
1 / 10	0.5	0.029	0.099	No	No	No
1 / 10	0.5	0.034	0.118	No	No	No
1 / 10	0.45	0.038	0.139	No	No	No
1 / 10	0.45	0.042	0.163	Yes	No	No
1 / 10	0.45	0.048	0.184	Yes	No	No
1 / 10	0.35	0.047	0.160	Yes	No	No
1 / 10	0.3	0.075	0.293	Yes	Yes	No
1 / 10	0.29	0.103	0.373	Yes	Yes	No
1 / 10	0.2	0.113	0.420	Yes	Yes	No
1 / 10	0.2	0.131	0.475	Yes	Yes	No
1 / 10	0.2	0.139	0.498	Yes	Yes	No
1 / 9.64*	unknown	0.350	0.873	Yes	Yes	Plunging
1 / 12	1.75	0.105	0.331	Yes	Yes	No

1 / 12	1.75	0.137	0.445	Yes	Yes	Surging
1 / 12	1.75	0.150	0.475	Yes	Yes	Surging
1 / 12	1.75	0.198	0.580	Yes	Yes	Plunging
1 / 20	0.34	0.005	0.018	No	No	No
1 / 20	0.34	0.008	0.027	No	No	No
1 / 20	0.34	0.011	0.033	No	No	No
1 / 20	0.34	0.016	0.051	No	No	No
1 / 20	0.34	0.020	0.066	Yes	No	No
1 / 20	0.34	0.025	0.081	Yes	No	No
1 / 20	0.34	0.030	0.099	Yes	No	No
1 / 20	0.27	0.028	0.102	Yes	No	No
1 / 20	0.27	0.040	0.135	Yes	Yes	No
1 / 20	0.27	0.050	0.172	Yes	Yes	Surging
1 / 20	0.27	0.060	0.192	Yes	Yes	Surging
1 / 20	0.27	0.080	0.237	Yes	Yes	Plunging
1 / 20	0.27	0.100	0.275	Yes	Yes	Plunging
1 / 20	0.16	0.094	0.241	Yes	Yes	Plunging
1 / 20	0.16	0.140	0.311	Yes	Yes	Plunging
1 / 20	0.16	0.186	0.381	Yes	Yes	Plunging
1 / 20	0.16	0.233	0.431	Yes	Yes	Plunging
1 / 20	0.16	0.250	0.449	Yes	Yes	Plunging
1 / 20	0.16	0.326	0.530	Yes	Yes	Plunging
1 / 20	0.16	0.373	0.571	Yes	Yes	Plunging
1 / 20	0.16	0.417	0.621	Yes	Yes	Plunging
1 / 20	0.14	0.100	0.250	Yes	Yes	Plunging
1 / 20	0.13	0.150	0.308	Yes	Yes	Plunging

1 / 20	0.14	0.201	0.377	Yes	Yes	Plunging
1 / 20	0.14	0.307	0.491	Yes	Yes	Plunging

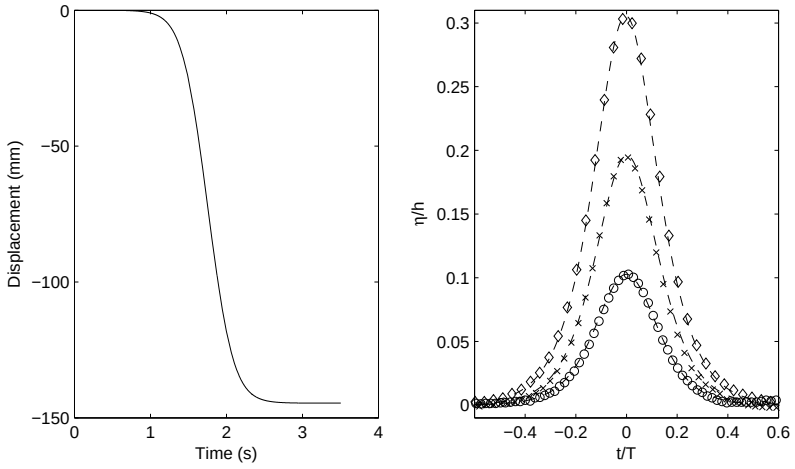

Figure 2.1: Left: a typical wave-maker trajectory to generate a $H/h = 0.2$ solitary wave in depth $h = 0.14\,m$; right: comparisons between experimental measurements in the $s = 1/20$ flume ($\circ \times \diamond$) and *Grimshaw*'s theoretical solutions of solitary waves with different H/h ratios (- - -).

Two successive solitary waves were also generated, by combining wave-maker trajectories of two individual solitary waves, with the crests of the two waves separated by a specified separation time. When the two solitary waves are close so that the two trajectories intersect each other, linear superposition of wave-maker velocity is applied, and the wave-maker trajectory is then found by integrating the combined velocity; the superposition process is illustrated in Figure 2.2. The two waves generated in such way are called "double solitary waves" herein.

For separation times $\tau/T > 0.47$, we are successful in generating two identical waves that maintain nearly permanent forms as they travel down the flume. Figure 2.3 shows an example of wave gauge records of double solitary waves

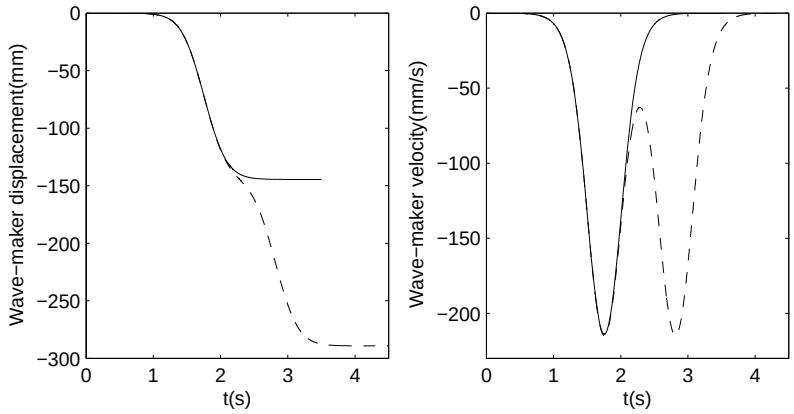

Figure 2.2: Comparison of wave-maker velocity and trajectory, between a single solitary wave and double solitary waves with separation time τ/T=0.6. H/h = 0.2 and h = 0.14 m. Left: wave-maker trajectory; right: wave-maker velocity. (—): single solitary wave; (- - -): double solitary waves.

at different locations. In this figure *Grimshaw*'s solitary wave solution is also plotted. Thus, the shortest separation time in the experiments reported herein is τ/T = 0.472. Table 2.3 and 2.4 tabulate the wave conditions for the double solitary waves.

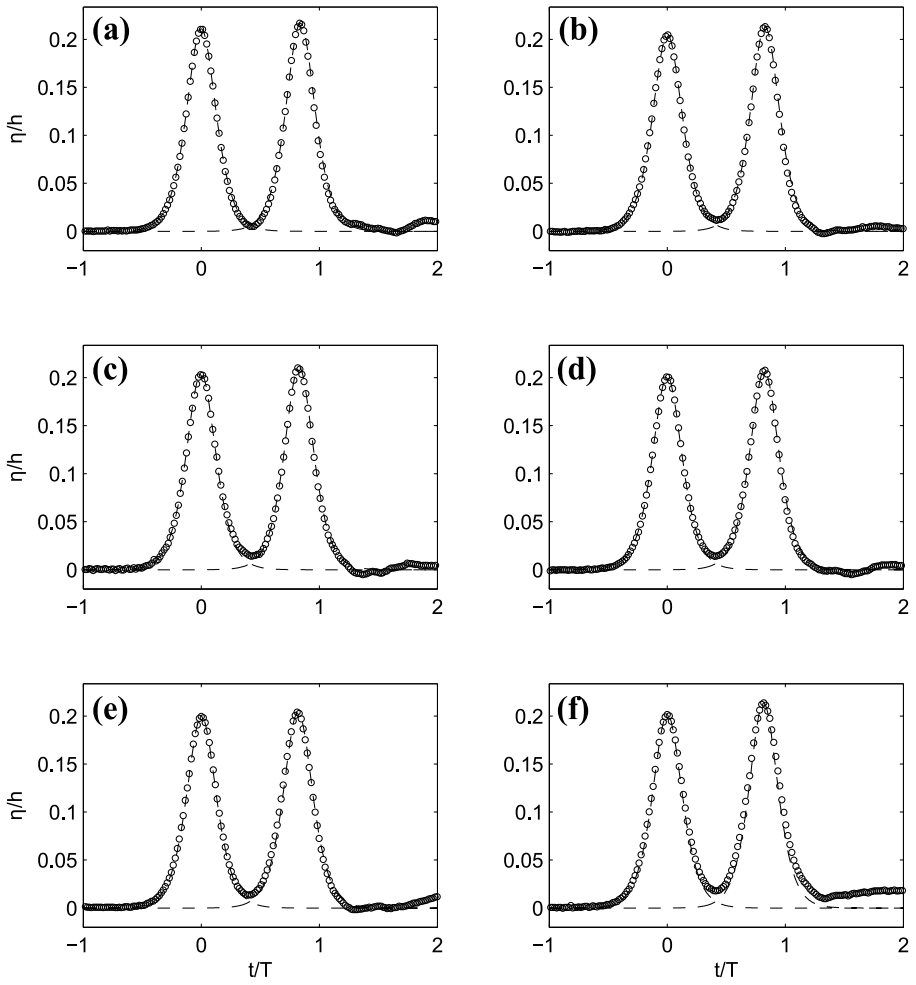

Figure 2.3: Wave gauge measurements of two successive solitary waves at different locations away from the wave-maker in the $s = 1/20$ flume at Cornell University. $\tau/T = 0.818$, $H/h = 0.201$. (a) The location of the wave gage is 3.62 λ away from the wave-maker; (b) 5.79 λ; (c) 7.12 λ (d) 7.95 λ (e) 8.80 λ (f) 9.73 λ (toe of the slope); (○): experimental data; (- - -): *Grimshaw*'s solution for a single solitary wave.

Table 2.3: A list of double solitary waves generated. *From *Raichlen* (unpublished data, 1985), which will be shown with present results herein.

Slope	Water depth h(m)	H/h	Separation time τ/T
1 / 2.47	0.2	0.101	0.525, 0.680, 0.864, 1.003, 1.176, 1.364, 1.528
1 / 2.47	0.2	0.202	0.678, 0.791, 0.852, 0.954, 1.123, 1.298, 1.466, 1.645
1 / 2.47	0.2	0.302	1.960, 1.635, 1.326, 1.221, 1.066, 0.816, 0.662
1 / 2.55*	unknown	0.225	1.020, 2.510
1 / 10	0.35	0.047	0.482, 0.565, 0.661
1 / 10	0.29	0.103	0.669, 0.801, 0.938, 1.212
1 / 10	0.2	0.139	0.866, 0.967, 1.179, 1.375, 1.577
1 / 9.64*	unknown	0.350	0.990, 1.231, 1.477, 1.723, 1.969, 2.221, 2.467
1 / 12	1.75	0.105	0.489, 0.611, 0.729, 1.016, 1.246, 1.525, 2.033
1 / 12	1.75	0.137	0.472, 0.716, 0.973, 1.231
1 / 12	1.75	0.150	0.570, 0.661, 0.709, 0.966, 1.205, 1.464, 1.990
1 / 12	1.75	0.198	0.549, 0.646, 0.700, 0.934, 1.434, 1.925
1 / 20	0.14	0.100	0.490, 0.570, 0.696, 0.860, 1.065, 1.294, 1.466, 1.669, 2.103, 2.451
1 / 20	0.13	0.150	0.636, 0.751, 0.918, 1.103, 1.233, 1.381, 1.605, 1.837, 2.013
1 / 20	0.14	0.201	0.637, 0.818, 1.015, 1.206, 1.496, 2.039, 2.616
1 / 20	0.14	0.307	0.685, 1.073, 1.507, 1.852, 2.183, 2.473, 3.114, 3.598, 3.920

Table 2.4: Experimental wave conditions of double solitary waves.

Slope	H / h	τ / T	R_1 / h	R_2 / h	Slope	H / h	τ / T	R_1 / h	R_2 / h
1 / 2.47	0.101	0.525	0.236	0.247	1 / 12	0.137	0.716	0.442	0.212
1 / 2.47	0.101	0.680	0.229	0.232	1 / 12	0.137	0.973	0.442	0.316
1 / 2.47	0.101	0.864	0.229	0.221	1 / 12	0.137	1.231	0.442	0.368
1 / 2.47	0.101	1.003	0.229	0.225	1 / 12	0.150	0.570	0.490	0.212
1 / 2.47	0.101	1.176	0.229	0.232	1 / 12	0.150	0.661	0.473	0.221
1 / 2.47	0.101	1.364	0.232	0.232	1 / 12	0.150	0.709	0.473	0.224
1 / 2.47	0.101	1.528	0.229	0.232	1 / 12	0.150	0.966	0.473	0.284
1 / 2.47	0.202	0.678	0.543	0.577	1 / 12	0.150	1.205	0.473	0.368
1 / 2.47	0.202	0.791	0.532	0.596	1 / 12	0.150	1.464	0.473	0.429
1 / 2.47	0.202	0.852	0.532	0.581	1 / 12	0.150	1.990	0.473	0.455
1 / 2.47	0.202	0.954	0.532	0.562	1 / 12	0.198	0.549	0.594	0.316
1 / 2.47	0.202	1.123	0.532	0.532	1 / 12	0.198	0.646	0.577	0.290
1 / 2.47	0.202	1.298	0.532	0.510	1 / 12	0.198	0.700	0.577	0.281
1 / 2.47	0.202	1.466	0.532	0.524	1 / 12	0.198	0.934	0.577	0.247
1 / 2.47	0.202	1.645	0.532	0.532	1 / 12	0.198	1.434	0.577	0.412
1 / 2.47	0.302	0.662	0.858	0.940	1 / 12	0.198	1.925	0.577	0.551
1 / 2.47	0.302	0.816	0.865	0.854	1 / 20	0.100	0.490	0.255	0.211
1 / 2.47	0.302	1.066	0.843	0.865	1 / 20	0.100	0.570	0.255	0.202
1 / 2.47	0.302	1.221	0.850	0.892	1 / 20	0.100	0.696	0.261	0.193
1 / 2.47	0.302	1.326	0.858	0.903	1 / 20	0.100	0.860	0.246	0.175
1 / 2.47	0.302	1.635	0.847	0.865	1 / 20	0.100	1.065	0.246	0.193
1 / 2.47	0.302	1.960	0.854	0.832	1 / 20	0.100	1.294	0.246	0.211

1 / 2.55	0.225	1.015	0.593	0.569	1 / 20	0.100	1.466	0.246	0.229
1 / 2.55	0.225	2.508	0.595	0.585	1 / 20	0.100	1.669	0.246	0.246
1 / 10	0.047	0.480	0.160	0.143	1 / 20	0.100	2.103	0.246	0.246
1 / 10	0.047	0.570	0.160	0.149	1 / 20	0.100	2.451	0.246	0.246
1 / 10	0.047	0.660	0.160	0.154	1 / 20	0.150	0.636	0.342	0.281
1 / 10	0.103	0.670	0.373	0.267	1 / 20	0.150	0.751	0.323	0.260
1 / 10	0.103	0.800	0.373	0.307	1 / 20	0.150	0.918	0.312	0.221
1 / 10	0.103	0.940	0.373	0.353	1 / 20	0.150	1.103	0.308	0.212
1 / 10	0.103	1.210	0.373	0.363	1 / 20	0.150	1.233	0.310	0.214
1 / 10	0.139	0.870	0.493	0.280	1 / 20	0.150	1.381	0.302	0.221
1 / 10	0.139	0.970	0.500	0.340	1 / 20	0.150	1.605	0.308	0.250
1 / 10	0.139	1.180	0.498	0.410	1 / 20	0.150	1.837	0.298	0.289
1 / 10	0.139	1.380	0.500	0.460	1 / 20	0.150	2.013	0.310	0.304
1 / 10	0.139	1.580	0.500	0.490	1 / 20	0.201	0.637	0.389	0.389
1 / 9.64	0.350	0.990	0.869	0.397	1 / 20	0.201	0.818	0.398	0.354
1 / 9.64	0.350	1.231	0.869	0.318	1 / 20	0.201	1.015	0.368	0.273
1 / 9.64	0.350	1.477	0.875	0.455	1 / 20	0.201	1.206	0.377	0.255
1 / 9.64	0.350	1.723	0.882	0.581	1 / 20	0.201	1.496	0.377	0.255
1 / 9.64	0.350	1.969	0.880	0.727	1 / 20	0.201	2.039	0.366	0.309
1 / 9.64	0.350	2.221	0.864	0.822	1 / 20	0.201	2.616	0.366	0.363
1 / 9.64	0.350	2.467	0.875	0.890	1 / 20	0.307	0.685	0.497	0.551
1 / 12	0.105	0.489	0.334	0.165	1 / 20	0.307	1.073	0.497	0.408
1 / 12	0.105	0.611	0.330	0.191	1 / 20	0.307	1.507	0.488	0.328
1 / 12	0.105	0.729	0.330	0.229	1 / 20	0.307	1.852	0.480	0.301
1 / 12	0.105	1.016	0.330	0.294	1 / 20	0.307	2.183	0.480	0.310
1 / 12	0.105	1.246	0.330	0.323	1 / 20	0.307	2.473	0.480	0.319

1/12	0.105	1.525	0.330	0.323	1/20	0.307	3.114	0.497	0.408
1/12	0.105	2.033	0.330	0.334	1/20	0.307	3.598	0.504	0.495
1/12	0.137	0.472	0.455	0.195	1/20	0.307	3.920	0.495	0.513

2.3 Wave height definition

Since single solitary waves in the experiments maintain constant wave shapes in the constant-depth region, the wave heights in the middle of the constant-depth region are reported herein as the incident wave heights. In the case of double solitary waves, the period and wavelength of the first wave are used for normalization.

For the cases of double solitary waves, two sources of uncertainty in wave heights exist. First, the two solitary waves within one experimental run can have wave heights that slightly deviate from each other and the specified value. Second, the wave heights across experimental runs with different separation times, can also vary, undermining the goal to treat wave heights as controls and separation times as variables. To show this variation in wave heights, Figure 2.4 shows the wave gauge measurements with four different separation times in the $s = 1/20$ flume. The resulting uncertainty in wave heights is determined as such: for a specific set of experiments with similar wave heights but different separation times, the average of all wave heights is seen as the overall wave height, and the maximum deviation from this wave height is considered to be the uncertainty associated with this set of experiments. With the above scheme, the maximum wave-height uncertainty associated with the double solitary waves experiments is found to be ± 0.012 (H/h), or $\pm 7.33\%$ of wave height. The com-

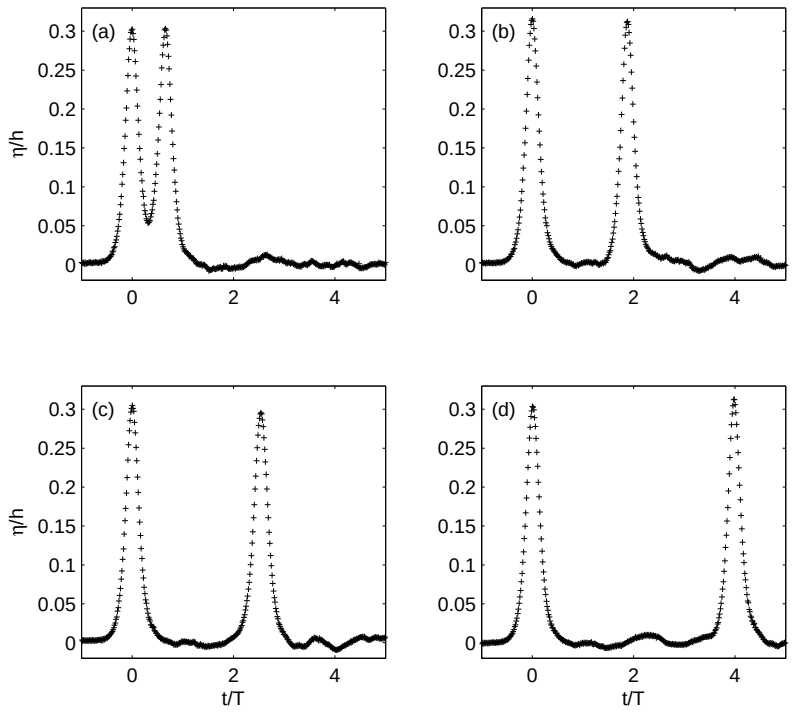

Figure 2.4: Double solitary waves measurements in the $s = 1/20$ flume at a fixed location from cases with four different separation times. τ/T = (a) 0.685; (b) 1.852; (c) 2.473; (d) 3.920.

plete wave height uncertainty table can be seen in Table 2.5.

2.4 Wave breaking conditions

To consistently classify whether waves break or not, a wave-breaking criterion is needed. *Synolakis* [1987] analytically derived a criterion for solitary wave breaking during run-up:

$$\frac{H}{h} > 0.8183\, s^{\frac{10}{9}} \quad \text{or} \quad s\left(\frac{H}{h}\right)^{-\frac{9}{10}} < (0.8183)^{-\frac{9}{10}}. \tag{2.1}$$

Table 2.5: Wave height uncertainty table for double solitary waves.

Slope	Overall H/h	Maximum H/h deviation	Maximum % deviation
1 / 2.47	0.101	±0.004	±3.96%
1 / 2.47	0.202	±0.009	±4.46%
1 / 2.47	0.302	±0.009	±2.98%
1 / 2.55	0.225	±0.005	±2.22%
1 / 10	0.047	±0.002	±4.26%
1 / 10	0.103	±0.005	±4.85%
1 / 10	0.139	±0.002	±1.44%
1 / 9.64	0.350	±0.010	±2.86%
1 / 12	0.105	±0.007	±6.67%
1 / 12	0.137	±0.006	±4.38%
1 / 12	0.150	±0.008	±5.33%
1 / 12	0.198	±0.009	±4.55%
1 / 20	0.100	±0.004	±4.00%
1 / 20	0.150	±0.011	±7.33%
1 / 20	0.201	±0.010	±4.98%
1 / 20	0.307	±0.012	±3.91%

Madsen and Schäffer [2010] recently proposed a more accurate criterion for solitary wave breaking during back-wash (*Gjevik and Pedersen* [1981] first derived a similar criterion using a half-sine single wave),

$$\frac{H}{h} > 0.5139\, s^{\frac{10}{9}} \quad \text{or} \quad s\left(\frac{H}{h}\right)^{-\frac{9}{10}} < (0.5139)^{-\frac{9}{10}}. \tag{2.2}$$

Note that on a given slope the back-wash breaking can occur for smaller incident waves compared to those for run-up breaking to occur. As *Synolakis*

pointed out himself, (2.1) may not be physical when compared to experimental observations. To be specific, (2.1) predicts wave breaking during run-up on a $s = 1/2.47$ slope for H/h greater than 0.3, yet no visible breaking occurred on this slope even when $H/h = 0.5$. Figure 2.5(a)(b)(c) shows a sequence of this wave running up the slope. It is clear that wave breaking was not visible during the run-up phase, but it did happen during the back-wash phase, (d). One possible explanation of such discrepancy between the theoretical prediction and laboratory observation lies in the way breaking is defined in the analytical sense - a wave breaks when the wave front becomes vertical (slope of free surface approaches infinity). However, a vertical wave front at an instant does not guarantee that the wave will break at the next instant. The base of the wave may accelerate and catch up smoothly with the crest before any broken free surface develops, thus preventing breaking from developing after a vertical wave front first appears. *Jensen et al.* [2003] discussed this issue in their experiments on a $s = 1/5.37$ slope during wave run-up, and illustrated the above process by PIV measurements. On the other hand, the breaking criterion during the back-wash phase, (2.2), appears highly consistent with laboratory observation - since the flow is now receding, soon after a vertical front develops it must collapse. Figure 2.5(d) is a snapshot of a back-wash breaking

Utilizing a fully non-linear potential flow model, *Grilli et al.* [1997] provided a breaking criterion based on numerically computed wave shapes. They defined the three breaker types as follows: spilling breaker type occurs when the vertical distance between the wave crest and the tip of the overturning jet is smaller than half the wave height right before the jet touches the free surface, plunging breaker type occurs when the distance is greater than half the wave height, and

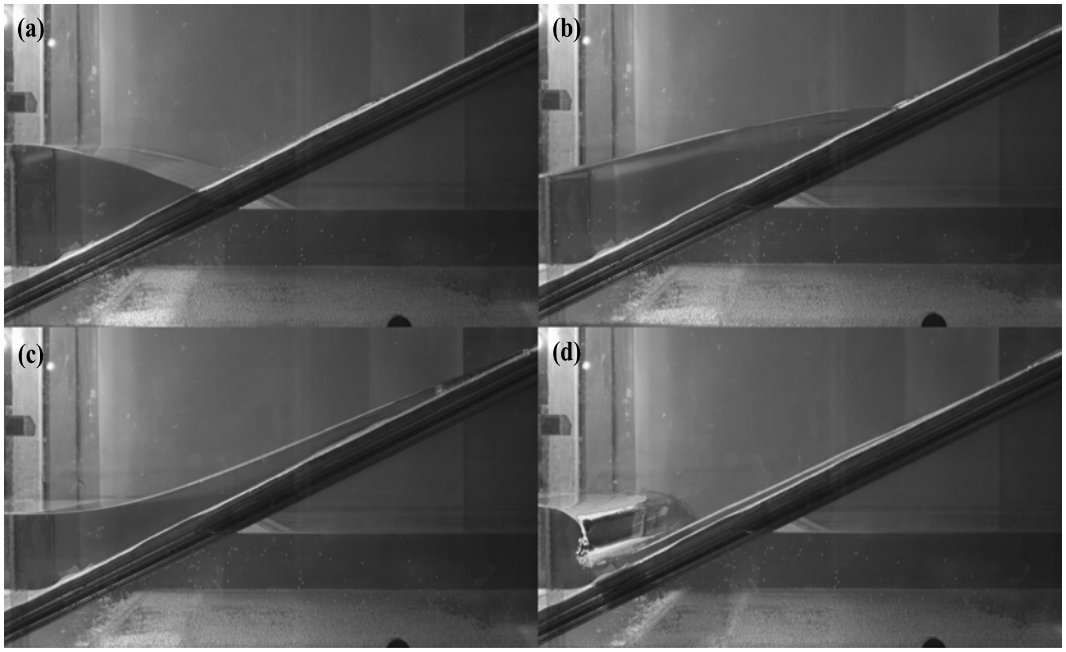

Figure 2.5: Sequence of a solitary wave with $H/h = 0.5$ running up a $s = 1/2.47$ slope. (a) The moment with the steepest run-up front; (b) the wave continues running up the slope; (c) maximum run-up; (d) right before the back-wash breaking occurs

surging breaker type occurs when the base of the wave becomes vertical.

With all the numerically computed cases, they recommended the following wave breaking criterion for solitary waves, where the breaking parameter is essentially the ratio of a characteristic wavelength to the horizontal slope length, as shown in (1.3):

$$S = 1.521\frac{s}{\sqrt{\frac{H}{h}}} = 0.419\frac{l}{L}\begin{cases} \text{No breaking, if } 0.37 < S \\ \text{Surging breaker, if } 0.3 < S < 0.37 \\ \text{Plunging breaker, if } 0.025 < S < 0.3 \\ \text{Spilling breaker, if } S < 0.025 \end{cases} \tag{2.3}$$

This criterion predicts that no breaking will occur on slopes steeper than $s = 1/4.7$, which agrees with our observations that no breaking occurred on the $s = 1/2.47$ slope. Overall, *Grilli et al.*'s criterion compares well with our ex-

perimental observations, whereas *Synolakis*' underpredicts the wave height for visible wave breaking to occur. We remark here that *Grilli et al.*'s criterion can be seen as an "empirical" criterion based on numerical experiments. The advantage of *Grilli et al.*'s criterion is that it is related to the wave shape, and numerically the breaker type can be specified without ambiguity.

2.5 Run-up measurements

The run-up front of single solitary waves or the first wave in the double solitary wave case generally assumes a parabolic shape with the two sides lower than the center, likely due to no-slip condition at the walls of the flume; on the other hand, for the second wave in the two-wave case, depending on the wave condition the second run-up assumes different shapes, which can be parabolic, inverse-parabolic, uniform, or ill-defined (nearly invisible). Figure 2.6 and Figure 2.7 show examples of different run-up shapes. Given the mostly non-uniform run-up shapes, it is important to specify how run-ups are reported. Two direct ways to describe run-up are: average (across the width of the flume) and maximum (the highest point of the run-up front) run-up.

To calculate average run-up, the location and shape of the entire run-up front need to be known. A run-up front tracing program was developed to determine average run-ups from recorded run-up videos. The program traces the run-up front by detecting temporal change in brightness at each pixel location in the run-up videos (at least 30 frames per second). Since from the grid lines marked on the slope the actual location of the pixels can be derived, the traced run-up

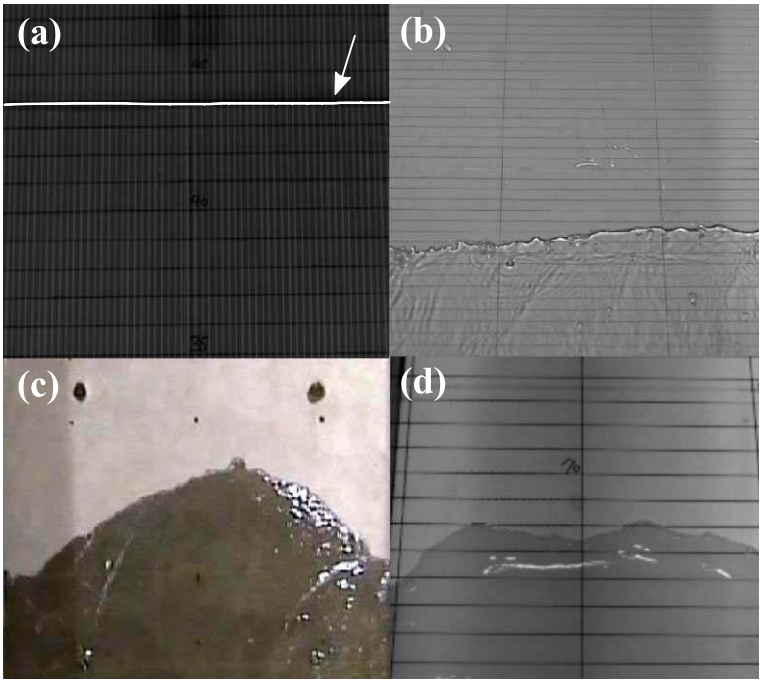

Figure 2.6: Single solitary wave run-up shapes. (a) s = 1/2.47 slope with glass surface; (b) s = 1/10 slope with glass surface; (c) s = 1/12 slope with concrete surface; (d) s = 1/20 slope with styrene surface.

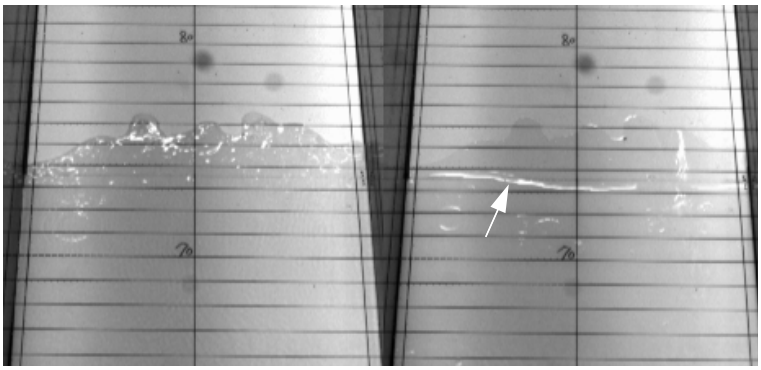

Figure 2.7: Double solitary wave run-up shapes. s = 1/20, H/h = 0.201, and τ/T = 0.818 (a) first run-up; (b) second run-up.

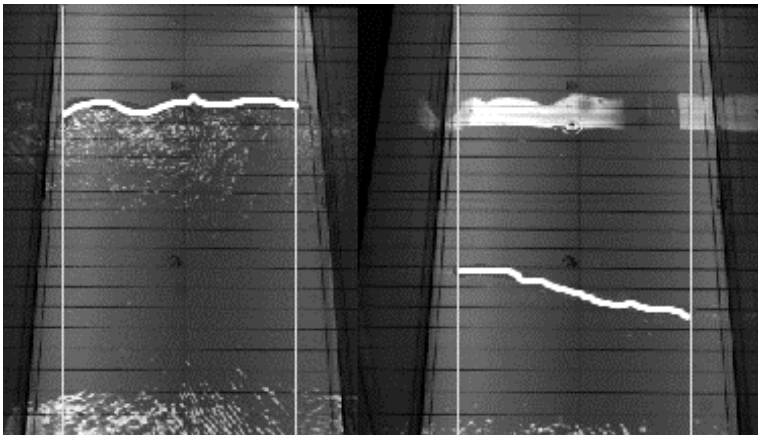

Figure 2.8: An example of program-traced run-up fronts. $s = 1/20$, $H/h = 0.307$, and $\tau/T = 1.852$ (a) program-traced first run-up; (b) program-traced second run-up.

front can then be averaged and the average run-up computed. An example of traced run-up fronts is shown in Figure 2.8. The tracing program works well when the run-up front is well-defined and easily distinguishable, as is the case with single wave run-ups or the first wave run-ups in the two-wave experiments. When the run-up front is ill-defined and less distinguishable, however, as is the case with most second wave run-ups, obtaining a continuous and physical run-up front requires excessive smoothing and manual filtering, which reduces the efficiency, objectiveness, and consistency associated with the program tracing method.

To determine maximum run-up, on the other hand, is much simpler. The following technique was employed to determine the maximum run-up: visually identify the maximum run-up location in the run-up video, and linearly interpolate between the nearest two known grid lines or fiducial marks to find the actual location of the maximum run-up.

Although reporting average run-ups seems the more logical choice to address non-uniform run-up shapes, average run-ups cannot be compared with the majority of existing data where maximum run-ups were reported, can be difficult to measure when the run-up front is not well-defined, and require a more sophisticated measurement technique (e.g. video camera and a program to trace and average the run-up front). Thus, to be consistent with existing run-up studies, in the rest of the discussion we will report maximum instead of average run-ups.

Nonetheless, it is worth pointing out how significantly average run-ups reduce discrepancies between experimental data. Based on his experimental data for breaking solitary waves, *Synolakis* [1987] computed empirical equations for both maximum and average run-ups:

$$\frac{R_{max}}{h} = 1.109\left(\frac{H}{h}\right)^{0.582} \tag{2.4}$$

$$\frac{R_{ave}}{h} = 0.918\left(\frac{H}{h}\right)^{0.606} \tag{2.5}$$

Figure 2.9 compares (2.4) and (2.5) to our data on the $s = 1/20$ slope. It can be observed that while noticeable discrepancy shows in maximum run-ups, average run-ups compare nicely, which also implies that the run-up fronts in our experiments are more uniform compared to those in *Synolakis'* experiments.

The uncertainty associated with the maximum run-up determination method can be estimated as follows: in facilities where grids on the slope were used, the grid lines have a thickness of about 2 mm, and so does the visible front of the run-ups. The uncertainty is therefore estimated to be ±2 mm on the slope. In the large-scale tank with $s = 1/12$ slope, where bolts on the slope, of diameter about

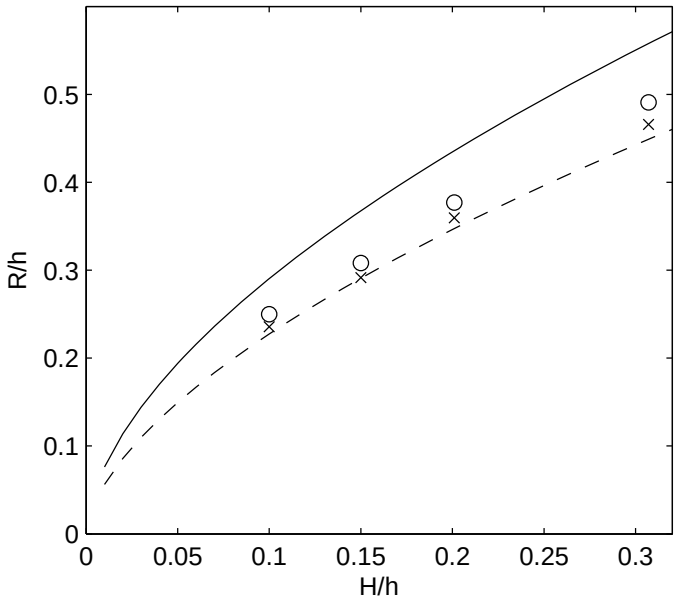

Figure 2.9: Comparison of maximum and average run-ups on a $s = 1/20$ slope. (—): *Synolakis'* maximum run-up (2.4); (- - -): *Synolakis'* average run-up (2.5); (○): our maximum run-up; (×): our average run-up.

5 cm, were used as fiducial marks, the uncertainty is therefore considered to be ±5 cm on the slope. Converted from length on the slope into vertical height and normalized by the lowest water depth used, the maximum uncertainty is found to be ±0.4% on the $s = 1/2.47$ slope. Table 2.6 lists the uncertainty associated for each laboratory setup. To ensure the method yields reasonably accurate run-up, parts of the run-up results are compared to those obtained by direct visual estimate and by the run-up tracing program; no significant difference shows.

Table 2.6: Uncertainty associated with run-up determination method.

Slope	Smallest depth	Uncertainty on the slope	Uncertainty in run-up height	Depth-normalized run-up uncertainty
1/2.47	0.20 m	±2 mm	±0.8 mm	±0.4%
1/10	0.20 m	±2 mm	±0.2 mm	±0.1%
1/12	1.75 m	±5 cm	±0.4 cm	±0.2%
1/20	0.13 m	±2 mm	±0.1 mm	±0.08%

2.6 Repeatability

The experiments show high degree of repeatability. More than half of the experiments were conducted at least twice; as shown in Figure 2.10, the measured surface elevations from repeated trials show nearly no discrepancy. To ensure accurate and consistent results, sufficient waiting time was allocated for the water in the flume to quiesce. The difference between the repeated runs, in terms of measured wave heights, run-ups, and separation times (in cases of double solitary waves), are ensured to be less than 1% before the data can be used.

2.7 PIV measurements

To gain further insights into the run-up processes, a set of PIV measurements (*Park* [2009]) was carried out on a $s = 1/20$ glass slope for both single and double solitary waves with $H/h = 0.15$ and $h = 13$ cm. The τ/T covered ranges from 0.656 to 1.892. The size of the field of view (FOV) of interest is 70 mm × 70 mm, set parallel to the sidewalls along the centerline of the wave tank, with

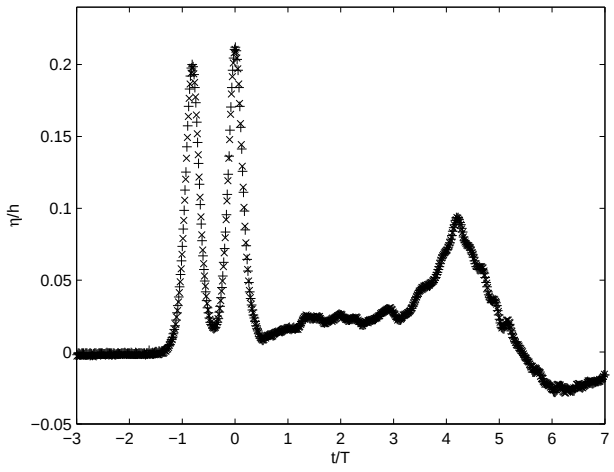

Figure 2.10: Complete wave gauge measurements including incident waves and reflected waves measured at the toe of the 1/20 slope, from two repeated runs with identical wave condition, $H/h=0.201$ and $\tau/T=0.818$. Each symbol represents measurement from one run.

the shoreward edge 100 mm away from the still-water shoreline along the slope (thus the FOV covers 100 mm to 170 mm offshore away from the initial shoreline). Fluorescent particles were used along with a Spectra Physics PIV400-30 Nd:YAG pulsed laser system to obtain PIV velocity field data at 15 Hz. Detailed description on the PIV setup and analysis has been discussed by *Park* [2009]. A total of three acoustic wave gages (Banner Engineering S18U) were used: one at the center of the FOV and the other two offshore (7 m and 8.2 m away from the toe of the slope) to measure the reflected waves.

CHAPTER 3

SINGLE SOLITARY WAVE

3.1 Solitary wave surf parameter

Numerous experimental and analytical studies of the run-up process of single solitary wave have been reported in the literature. These studies have covered a wide range of beach slopes, beach materials, and wave-height-to-water-depth ratios. As has been discussed in Section 1.3, for non-breaking solitary waves over a plane beach, based on the condition given in (2.1), *Synolakis* [1987] derived a run-up height expression in terms of an integral involving Bessel functions, (1.11). The approximate theory *Synolakis* adopted requires the amplitude of incident solitary wave be small in the constant depth region. For $s^{-1}\sqrt{H/h} \gg 0.288$ *Synolakis* further simplified the run-up integral and obtained the run-up law:

$$\frac{R}{h} = 2.831 s^{-\frac{1}{2}} \left(\frac{H}{h}\right)^{\frac{5}{4}}. \tag{3.1}$$

On the other hand, for breaking solitary waves, *Hsiao et al.* [2008] incorporated experimental run-up data on slopes ranging from $s = 1/15$ to $s = 1/60$, and proposed an empirical formula:

$$\frac{R}{h} = 7.712 s^{0.632} \sin^{0.618}\left(\frac{H}{h}\right). \tag{3.2}$$

By comparing (3.1) with (3.2), one immediately notices the opposite sign in the power of s, clearly indicating the difference in the run-up processes of breaking and non-breaking solitary waves.

In the conventional run-up height equations as shown in (3.1) and (3.2), the run-up height is normalized by the constant water depth, h. Alternatively, one can use the incident wave height, H, as the normalization factor, and express R/H as a function of H/h and s. Normalizing R by H gives a dynamic relation that better reflects the change in run-up heights: namely, a fixed value of R/H inherently implies that the larger the wave amplitude H, the larger the run-up height R. The disadvantage of using R/H, especially for small waves, is that experimental error can be greatly amplified, since both R and H are measured values with greater uncertainty compared to the still-water depth h.

The surf parameter for periodic waves, which has been widely used to seek similarity in wave breaking (*Galvin* [1968]) and run-up (*Battjes* [1974]), can be expressed as

$$\xi_p = s\left(\frac{H}{\lambda_p}\right)^{-\frac{1}{2}} = \frac{sT_p}{\sqrt{2\pi}}\sqrt{\frac{g}{H}}, \tag{3.3}$$

where λ_p is the wavelength and T_p the wave period of the periodic wave in deep water. Although the parameter was originally proposed empirically by *Iribarren and Nogales* [1949], *Mei* [1989] showed that the surf parameter can be analytically deduced from *Carrier and Greenspan*'s [1958] theory of the wave breaking criterion for a standing wave on a slope; the surf parameter is obtained by simply rearranging the analytical wave breaking criterion.

Kobayashi and Karjadi [1994] and *Fuhrman and Madsen* [2008] extended the concept of surf parameter for periodic waves to solitary wave. By proposing different ways to evaluate the wave period for a solitary wave in (3.3), they have suggested different forms of surf parameter for solitary wave. For example, *Fuhrman and Madsen* [2008] recommended that the surf parameter can be ob-

tained by using the effective wave period, (1.2), in (3.3), and find

$$\xi_{FM} = s\left(\frac{H}{h}\right)^{-1}, \tag{3.4}$$

in which the wave celerity has been approximated to be $c \sim \sqrt{gh}$. They demonstrated that the experimental breaking wave data cited in their paper collapsed onto the following empirical curve for the normalized run-up height

$$\frac{R}{H} = 3.9(\xi_{FM})^{0.42}. \tag{3.5}$$

However, to formally extend the surf parameter for periodic waves to solitary waves, we propose herein a different argument. Since *Mei* [1989] has shown that the surf parameter is linked to the wave breaking criterion, the same approach should be taken for solitary waves. As has been reviewed in Section 1.3, the solitary wave breaking criteria (2.2) and (2.1) have already been theoretically derived in ways similar to *Mei*'s for periodic waves, i.e., they are based on *Carrier and Greenspan*'s [1958] theory. Thus, from (2.2) and (2.1) the fundamental form of the surf parameter for solitary waves can be deduced as

$$\xi_s = s\left(\frac{H}{h}\right)^{-\frac{9}{10}}. \tag{3.6}$$

We note that surf parameter given in (3.6) is similar to that given by *Fuhrman and Madsen* [2008] in (3.4); only the powers of (H/h) are slightly different. However, the present definition does have a stronger theoretical foundation and requires less approximation. We further note that the surf parameter for solitary wave can be rewritten in terms of the horizontal length ratio and vertical length ratio as

$$\xi_s = \frac{\sqrt{3}}{2\pi}\left(\frac{l}{L}\right)\left(\frac{H}{h}\right)^{-\frac{2}{5}}, \tag{3.7}$$

in which (1.3) has been used.

3.2 Experimental results

The single solitary wave run-up results in terms of R/h is tabulated in Table 2.2. In Figure 3.1, single solitary wave run-up R/H is plotted against ξ_s^{-1}. Experimental data for both breaking and non-breaking solitary waves, including new results from the present experiments, are plotted. The theoretical breaking criterion (2.1) is also indicated. Given the definition of ξ_s, for a fixed depth h, a larger ξ_s^{-1} suggests a milder slope or a larger wave height. For small ξ_s^{-1}, waves do not break and are reflected - the smaller the ξ_s^{-1} the stronger the reflection from the slope. Thus, smaller ξ_s^{-1} gives smaller R/H. On the other hand, for large ξ_s^{-1}, the larger the ξ_s^{-1} the stronger the energy dissipation due to wave breaking. Thus, larger ξ_s^{-1} gives smaller R/H. Between the small and the large must exist a ξ_s^{-1} that corresponds to a maximum R/H - namely, a ξ_s^{-1} that corresponds to a nearly-breaking wave with minimum reflection from the slope. The run-up of breaking waves (to the right of the dashed-line in the figure) can be more or less collapsed with the surf parameter as already suggested by *Kobayashi and Karjadi* [1994] and *Fuhrman and Madsen* [2008]. Based on our surf parameter ξ_s, a simple curve-fit equation similar to (3.1) can be computed:

$$\frac{R}{H} = 4.1(\xi_s)^{0.43}. \tag{3.8}$$

The result is shown in Figure 3.1 and Figure 3.2. We note that although we included more experimental data and adopted a slightly different definition for the surf parameter, (3.1) and (3.8) are very similar.

For non-breaking waves additional slope dependency shows. To illustrate the slope dependency, the run-up integral (1.11), the run-up law (3.1), and experimental data are compared on slopes $s = 1/2.08$, $s = 1/10$, and $s = 1/20$, as shown in Figure 3.3.

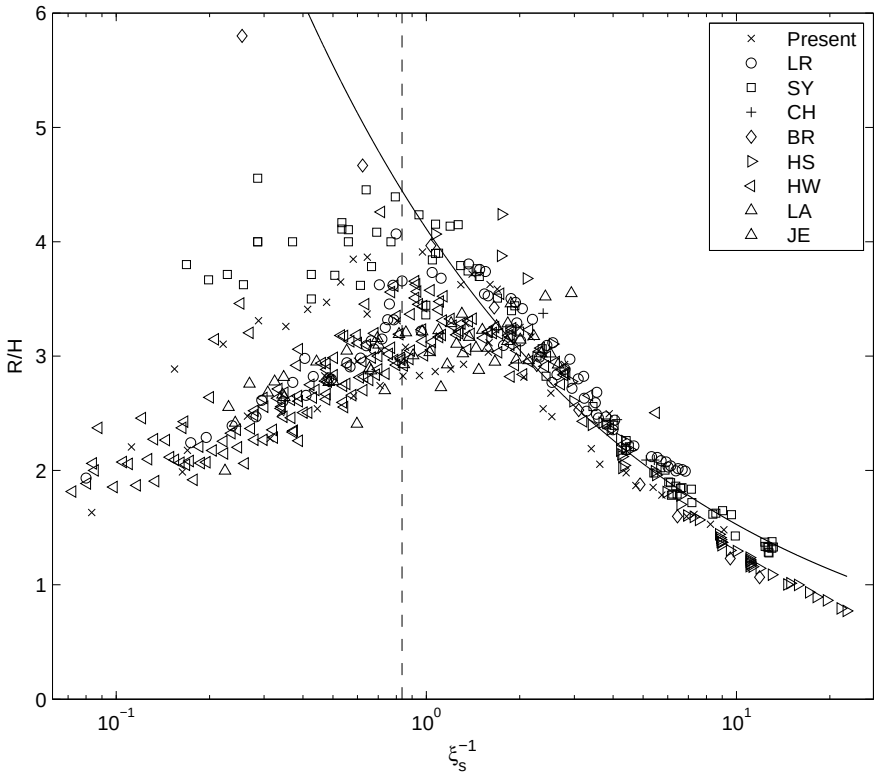

Figure 3.1: Unified single solitary wave run-ups. Only experimental data are included. LR: *Li and Raichlen* [2001, 2002]; SY: *Synolakis* [1987]; CH: *Chang et al.* [2009]; BR: *Briggs et al.* [1995]; HS: *Hsiao et al.* [2008]; HW: *Hall and Watts* [1953]; LA: *Langsholt* [1981]; JE: *Jensen et al.* [2003]; (- - -): wave-breaking criterion (2.1), waves break for ξ_s^{-1} larger than this threshold; (—) curve-fit (3.8)

We note that our data on the $s = 1/20$ slope are consistently lower than *Synolakis'* and *Chang et al.'s*. Efforts have been made to ensure this discrepancy is not a result of experimental misconduct. However, to show that for small waves R/H greatly amplifies experimental error, we can use the resolution of measurement to estimate the error bar for each data point. As discussed previously, the resolution of our data in the $s = 1/20$ tank is 0.2 mm in R (hence $R_{res} = 0.2$ mm) and 0.5 mm in H (hence $H_{res} = 0.5$ mm). The following scheme is used to conservatively estimate the upper $(R/H)_u$ and lower limits $(R/H)_l$ of the error bar

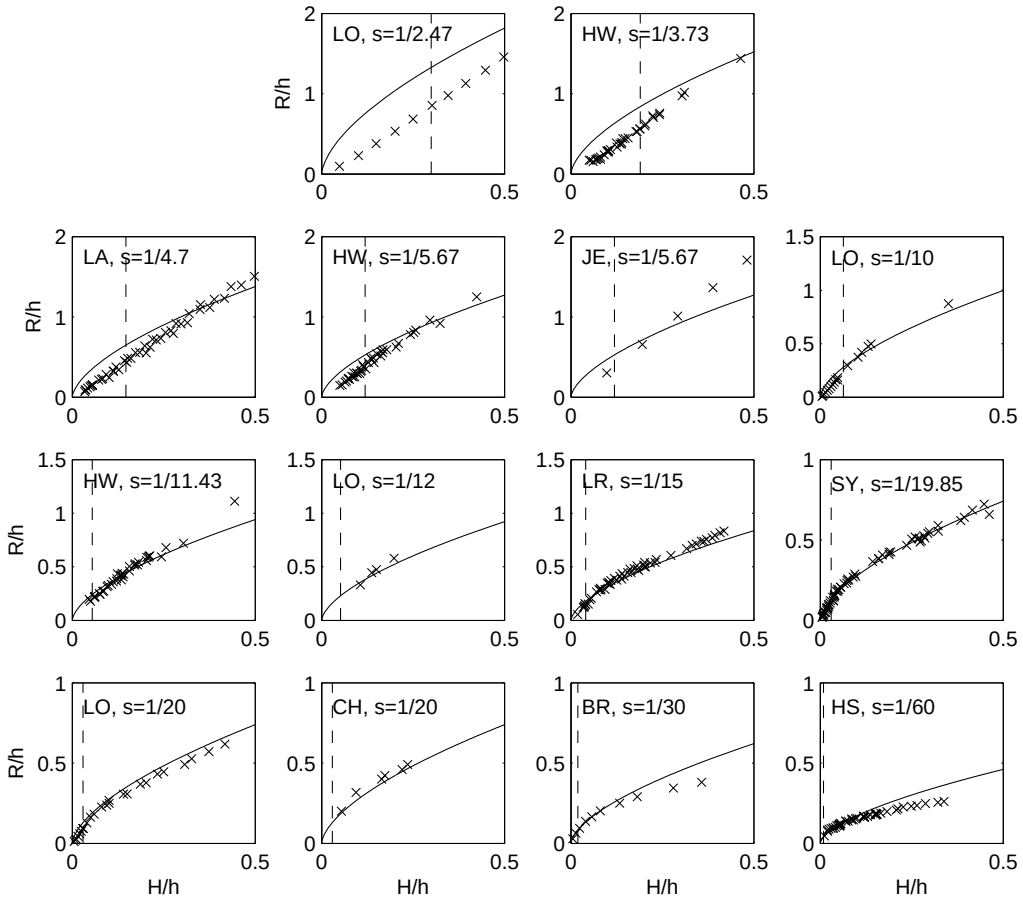

Figure 3.2: Experimental solitary wave run-ups and curve-fit (3.8), in terms of R/h. LR: *Li and Raichlen* [2002]; SY: *Synolakis* [1987]; CH: *Chang et al.* [2009]; BR: *Briggs et al.* [1995]; HS: *Hsiao et al.* [2008]; HW: *Hall and Watts* [1953]; LA: *Langsholt* [1981]; JE: *Jensen et al.* [2003]; LO: present study; (—): curve-fit (3.8); (- - -): wave-breaking criterion (2.1), the curve-fit is applicable to the right of this threshold.

centered at the reported value (R_r/H_r):

$$(\frac{R}{H})_u = \frac{R_r + R_{res}}{H_r - H_{res}}, \quad \text{and} \quad (\frac{R}{H})_l = \frac{R_r - R_{res}}{H_r + H_{res}}. \tag{3.9}$$

The result is shown with *Synolakis*' [1989] data in Figure 3.4 in terms of H/h

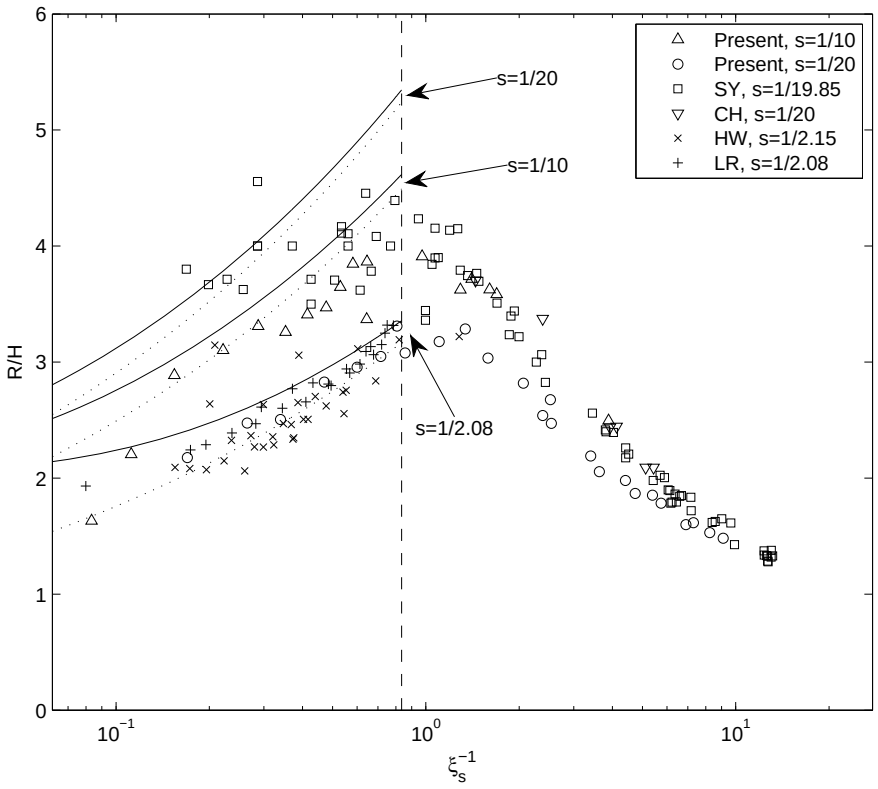

Figure 3.3: Single solitary wave run-ups on $s = 1/2.08$, $s = 1/10$, and $s = 1/20$ slopes only. (—): run-up integral (1.11); (· · ·): run-up law (3.1); (- - -): wave-breaking criterion (2.1), waves break for ξ_s^{-1} larger than this threshold.

against R/H (we note that *Synolakis* did not explicitly point out the resolution of measurement associated with his experiments, but he did point out that he could measure H as small as 1 mm and R was measured 1 mm above the slope). It can be observed that the error bar is much bigger for smaller waves than for bigger waves, again reminding us of how sensitive the dimensionally small waves are to the resolution of measurement, and dimensionally how small the seemingly large discrepancy between the two data set really is.

Despite the discrepancy, both the theory and experimental data consistently

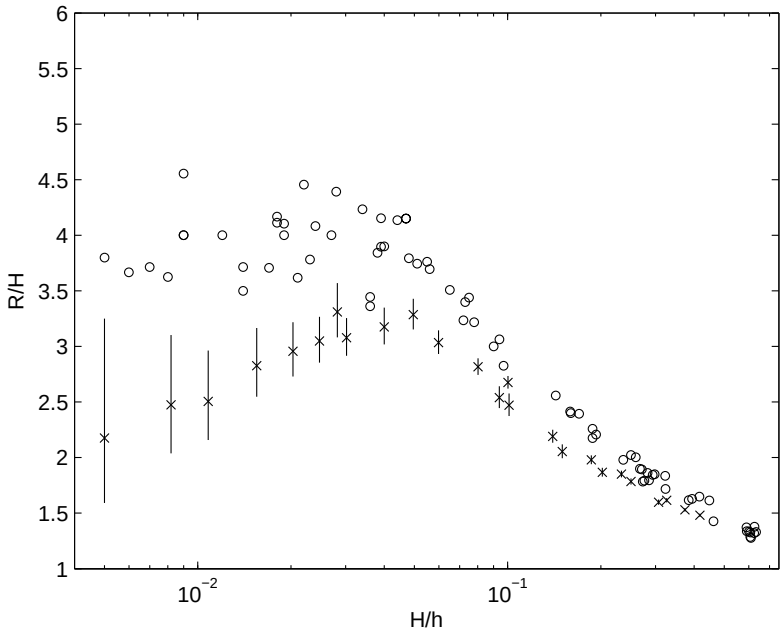

Figure 3.4: Error bars associated with single solitary wave run-up data. (×): our reported data on $s = 1/20$ slope; (—): estimated error bar associated with our data; (○): *Synolakis' [1987]* reported data on $s = 1/19.85$ slope.

show that for non-breaking waves R/H increases monotonically as ξ_s^{-1} increases, whereas for breaking waves the run-up peaks near the transition region. These observations suggest that a maximum R/H can be found by computing the R/H from the run-up law at the breaking limit, namely, $R/H = 2.831 s^{-\frac{1}{2}} (H/h)^{\frac{1}{4}}$ where $H/h = 0.8183 s^{\frac{10}{9}}$, which gives

$$\frac{R}{H} = 2.693 s^{-\frac{2}{9}}. \tag{3.10}$$

Using this method to predict the maximum fractional run-up (R/H) on a given slope can be useful when a quick and easy design estimate is needed.

While the wave-breaking condition may be inferred from the run-up trend, no detailed experimental measurements of actual wave shapes are available for

use to consistently classify breaker types. As an alternative, we classify wave breaking using *Grilli et al.*'s criterion (2.3), with the belief that the criterion incorporates information on the wave shapes before breaking occurs. The result is shown in Figure 3.5. In general, the breaker types based on (2.3) appear consistent with the run-up trend, with surging and plunging breakers on the right of the peak, non-breaking waves on the left, and a non-breaking-to-breaking transition zone near the peak. Overlaps exist near the transitions between each breaker type, which can be explained. As *Grilli et al.* pointed out in their own study, the classification of breaker types is arbitrary and can never be exact; they specified their definitions so that they could compute a consistent breaking criterion. *Mei* [1989] also reminded us that the transition from one breaker type to another is always gradual, and precise threshold values cannot be defined. In Figure 3.5 the analytical breaking criterion (2.1) is also marked in terms of ξ_s^{-1}; it is not surprising to see that the wave-breaking threshold is to the left of the peak, since we know (2.1) underestimates the wave height and slope mildness required for wave breaking, when compared to experiments. It is also interesting to see that the breaking wave data based on *Grilli et al.'s* criterion (2.3) are nicely collapsed by the solitary wave surf parameter. Having inspected Figure 3.5, we note that experimental solitary wave run-up data on slopes milder than $s = 1/60$ are lacking. To be exact, no experimental run-up data of spilling solitary waves based on (2.3) are available. While setting up such experiments is difficult due to limited tank length, information on spilling solitary wave run-ups is needed in order to complete the picture of solitary wave run-ups.

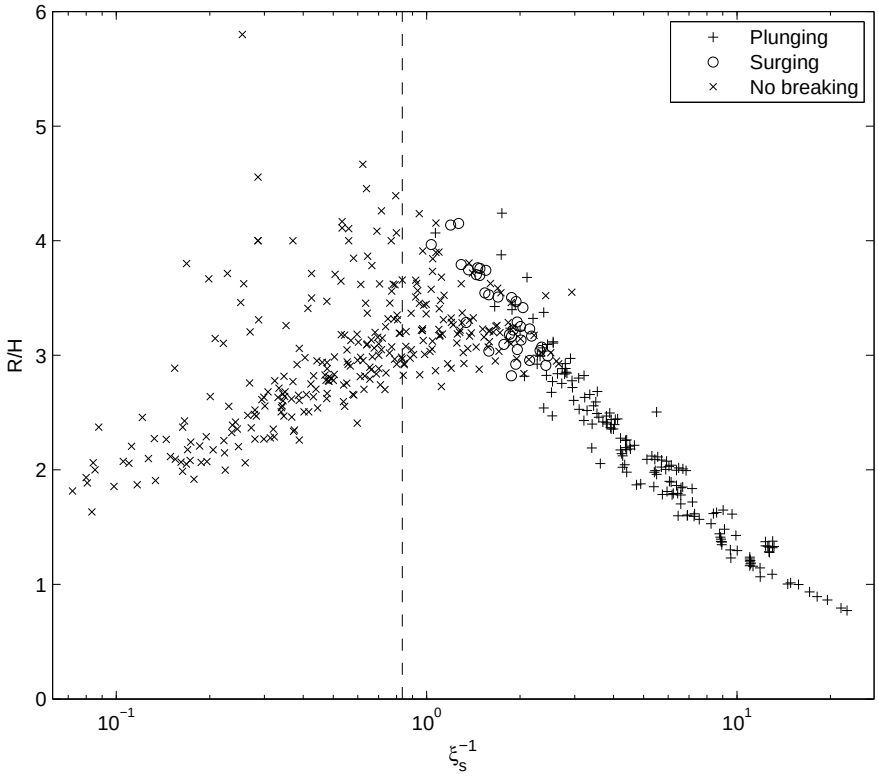

Figure 3.5: Wave breaking conditions of solitary wave data, based on (2.3). (- - -): breaking criterion based on (2.1), waves break for ξ_s^{-1} larger than this threshold.

CHAPTER 4

DOUBLE SOLITARY WAVES

4.1 Experimental results

All double solitary wave run-up results are plotted in Figure 4.1 and Figure 4.2, and tabulated in Table 2.4. In general, the run-ups caused by the first wave are not affected by the second solitary wave, regardless of the separation time, τ/T, and are the same as single solitary wave run-ups. The slight variation in the first run-ups are likely due to the uncertainty in wave heights, which has been discussed previously. However, for very short separation times, the first run-ups appear to increase slightly. In such cases the two wave heights at the toe of the slope are double-checked to ensure this slight increase is not a result of a larger first wave. Despite the observation, this trend is small and less significant when compared to the trend of the second run-ups. Thus, the rest of the discussion will focus on the second run-ups. On the $s = 1/10$, $s = 1/12$, and $s = 1/20$ slopes, the second run-ups assume a "spoon-shaped" trend. To make the results more readable and emphasize the trend, plots with second run-ups normalized by first run-ups are provided in Figure 4.3. When the separation time is long, as one would expect, the second run-up is identical to the first, since the two waves are separated long enough so that the interference between them is minimum. As the separation time shortens, the second run-up first decreases until a point of lowest run-up, and then the second run-up increases with respect to decreasing separation time, and eventually become the same as, or even higher than, the first run-up. A higher second run-up is observed in one case with $H/h = 0.307$ on the $s = 1/20$ slope. Although only one case yields

significantly higher second run-up, extra attention was paid to this particular case, to ensure the two wave heights are similar at the toe of the slope and that no mistakes were made in calculating the two run-ups, thus excluding the possibility of a severe experimental error. On the other hand, no similar trend show on the $s = 1/2.47$ slope. Figure 4.2 shows the results on the $s = 1/2.47$ slope.

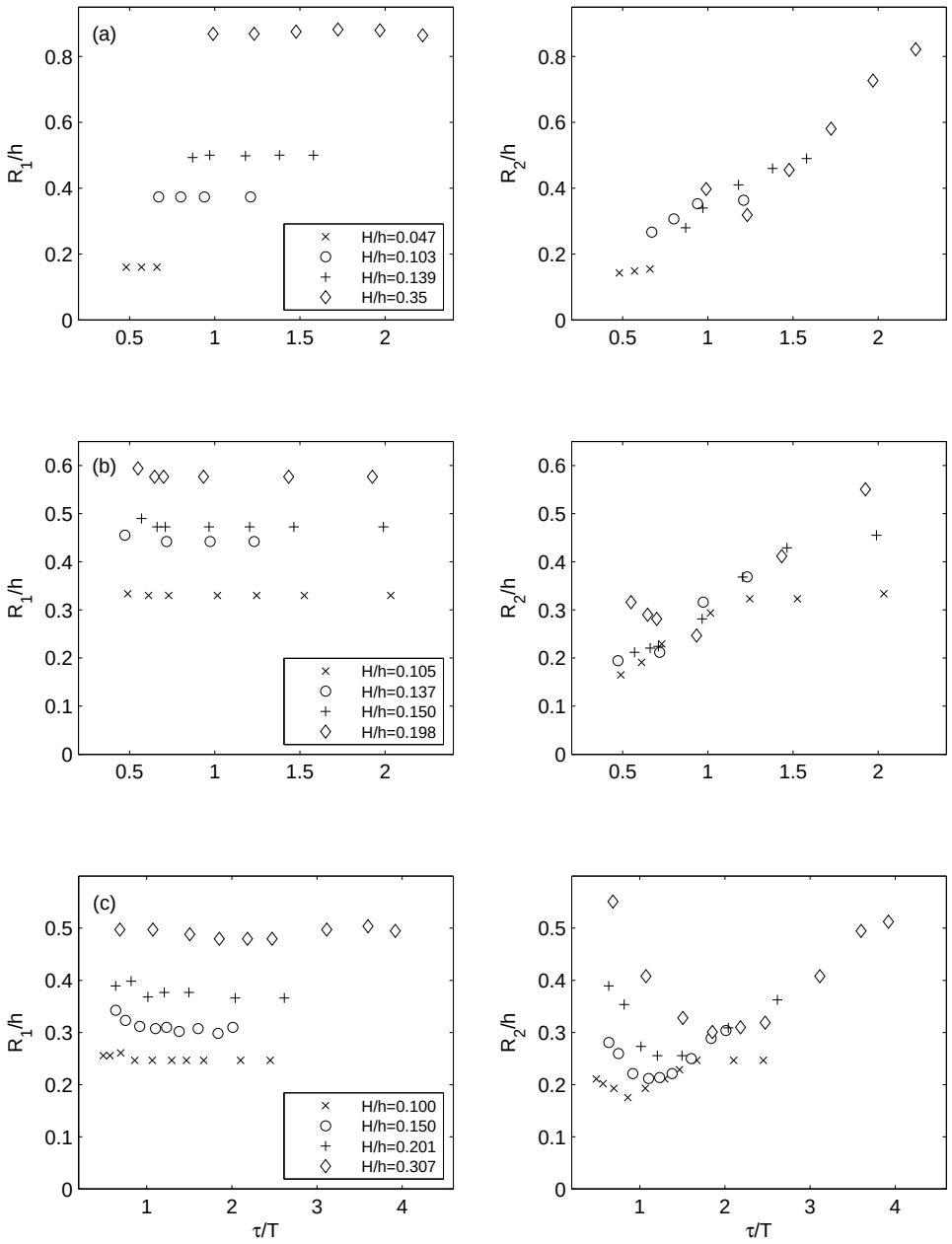

Figure 4.1: Double solitary wave run-ups on (a) s = 1/10 slope; (b) s = 1/12; (c) s = 1/20. Left panel: first run-up; right panel: second run-up.

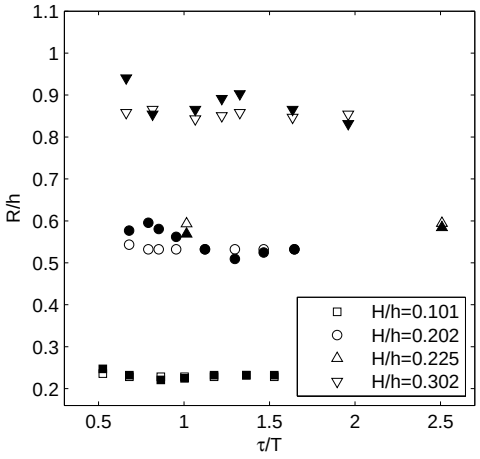

Figure 4.2: Double solitary wave run-ups on $s = 1/2.47$ slope. (□ ∘ △▽): first run-up; (■ ● ▲▼): second run-up.

We use the solitary wave surf parameter (3.7) to seek similarity in the run-ups of double solitary waves. By extending the single-wave analysis to the two-wave case, for double solitary waves the effective length of the wave front l becomes half the separation distance between the wave crests. For a fixed water depth solitary waves travel at constant speed, and therefore the separation length and separation time τ can be converted easily. With the new definition for l, the solitary wave surf parameter ξ_s becomes:

$$\xi_s = \frac{\sqrt{3}}{2\pi}\left(\frac{l}{L}\right)\left(\frac{H}{h}\right)^{-\frac{2}{5}} = s\left(\frac{H}{h}\right)^{-\frac{9}{10}}\left(\frac{\tau}{T}\right). \tag{4.1}$$

For double solitary waves, extra terms to rescale the run-ups are needed to collapse the data. The scattering of data can be reduced by introducing a $s^{-\frac{7}{6}}$ term, and the following curve-fit can be computed:

$$\Gamma = \left(\frac{R_2}{R_1} - 1\right)s^{-\frac{7}{6}} = f(\xi_s) = \frac{175\xi_s^{-0.22} - 199\xi_s^{-0.16}}{1 + 168\xi_s^{5.5}}. \tag{4.2}$$

The collapsed data and the curve-fit are plotted in Figure 4.4. Equation (4.2) can be rearranged to calculate R_2/R_1 directly:

$$\frac{R_2}{R_1} = f(\xi_s)s^{\frac{7}{6}} + 1. \tag{4.3}$$

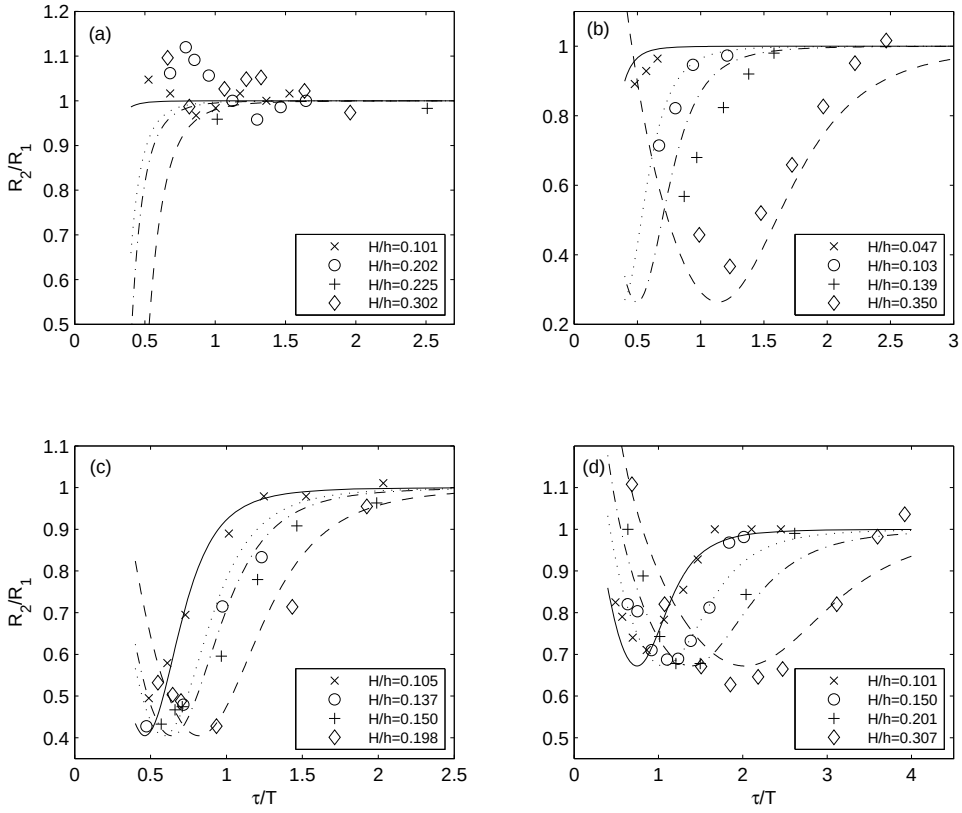

Figure 4.3: Double solitary wave run-ups in terms of R_2/R_1 on different slopes. (a) $s = 1/2.47$; (b) $s = 1/10$; (c) $s = 1/12$; (d) $s = 1/20$. (—): curve-fit (4.3) for (×); (· · ·): curve-fit for (○); (- · -): curve-fit for (+); (- - -): curve-fit for (⋄).

The curve-fit plotted in terms of R_2/R_1 against τ/T on different slopes is shown in Figure 4.3. We remark that while the solitary wave surf parameter ξ_s characterizes well the run-up trend in terms of separation time (or separation distance), it does not capture well the run-up heights. As a result, arbitrarily-chosen curve-fitting terms such as $s^{-\frac{7}{6}}$ were needed to rescale the run-ups, rendering (4.2) and (4.3) merely curve-fitted functions that may not possess much physical significance.

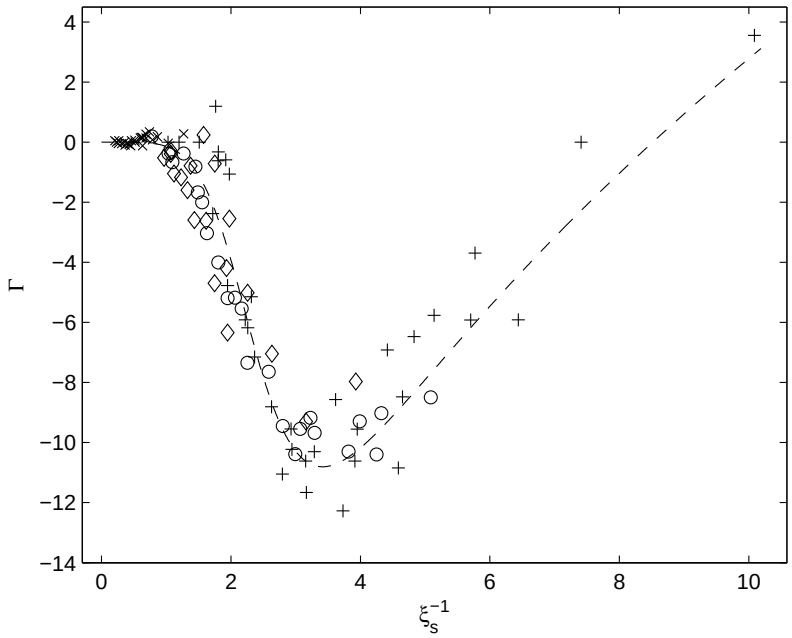

Figure 4.4: Collapsed experimental double solitary wave run-up data based on (4.2). (×): $s = 1/2.47$ slope; (⋄): $s = 1/10$ slope; (○): $s = 1/12$ slope; (+): $s = 1/20$ slope; (- - -): curve-fit (4.2).

4.2 Back-wash breaking

The back-wash breaking of the first wave appears to act as a great visual indicator of the regime the second run-up is in - we define regime I as where R_2 decreases with respect to increasing τ/T, and regime II as where R_2 increases with respect to increasing τ/T. Figure 4.5 shows a run-up snapshot of multiple $H/h = 0.307$ cases on the $s = 1/20$ slope, with the time origins synchronized (we note that the shiny areas near (b) and (d) are reflections of light; they do not affect the determination of the run-up fronts). As shown in the figure, the back-wash breaking, indicated by (a), of the first wave can be seen in cases where $\tau/T \geq 2.183$. For cases with $\tau/T < 2.183$, the second wave arrives before the first back-wash breaking occurs. In the case $\tau/T = 1.852$, the second wave arrives

almost at the same time the first back-wash breaking is about to form, and interestingly this case also produces the lowest second run-up. This relation on timing of the back-wash breaking and lowest run-ups holds for different H/h and on different slopes, suggesting that second waves arriving after the formation of the first back-wash breaking cause regime-II run-ups, whereas those arriving before the formation cause regime-I run-ups.

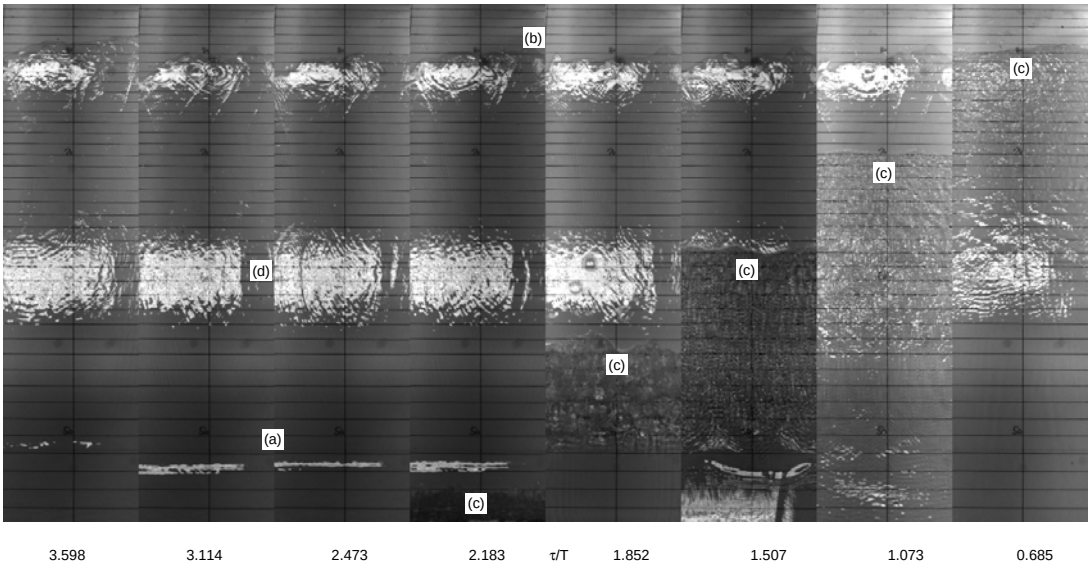

Figure 4.5: Synchronized double solitary wave run-up snapshot with $H/h = 0.307$ on a $s = 1/20$ slope for different separation times, τ/T. The waves travel upwards in the picture. (*a*): the shiny line, present in $\tau/T \geq 2.183$, is the back-wash breaking caused by the first wave; (*b*): water mark of the first run-up, present in all cases; (*c*): the second wave still running up the slope. The shiny areas near (*b*) and (*d*) are merely reflections of light that do not affect run-up determination.

The back-wash breaking is essentially a transient hydraulic jump, with the run-down flow receding rapidly from the shore, towards a pool of relatively calm water. The formation of a hydraulic jump indicates the peaking of this process, where the velocity difference between the two regions of flow reaches

its maximum. Since at this moment the receding flow is at its strongest stage, the second run-up is the lowest if the second wave arrives at the same time. Second waves arriving at a different moment will face a returning flow not as strong, thus causing higher run-ups and producing the observed spoon-shaped run-up trend. For very short separation time where the second wave arrives even before the first wave starts to recede, a second run-up higher than the first is possible, since it benefits from the still-shoreward-going momentum generated by the first run-up. On the steep $s = 1/2.47$ slope where the spoon-shaped trend isn't seen experimentally, the returning flow recedes much faster and the whole process ends within the time scale $0.47\,T$, while the adopted wave-generation mechanism only allows generation of two waves with $\tau/T > 0.47$. As a result, it cannot be concluded whether or not the spoon-shaped trend exists on steeper slopes (we also note that waves did not break during run-up on the $s = 1/2.47$ slope). On the other hand, from observation the back-wash breaking on the $s = 1/2.47$ slope is significantly more intense than those on the milder slopes, causing a greater disturbance in surface elevation near the shoreline. Thus, the slight variation in the second run-ups on the $s = 1/2.47$ slope is likely a result of this disturbance, whose effect is negligible on milder slopes.

4.3 PIV

The above process can be further illustrated by PIV measurements on double solitary waves on a $s = 1/20$ slope. We note that during the PIV experiments run-ups were not measured; the run-ups were measured in separate experiments with slightly different separation times. However, the range of the separation times for these two sets of experiments is the same (see Figure 4.6). For

easy reference, the eight separation times used in the PIV experiments are identified by letters A-H, as shown in the figure.

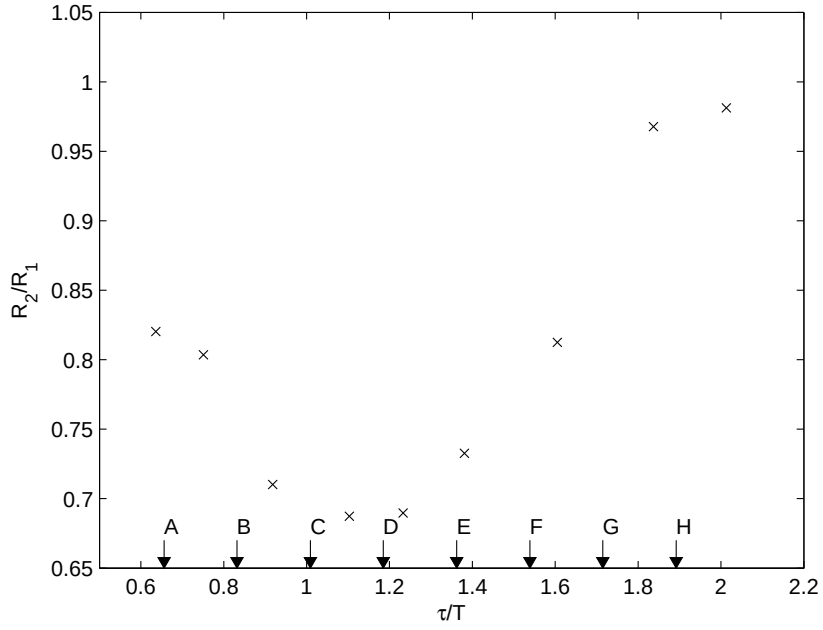

Figure 4.6: The separation times for PIV experiments and run-up measurements. (×): run-up measurements; (↓): separation times where PIV data are available. For easy reference, the PIV cases are labelled by letters A-H.

PIV images from three cases will be considered here: case A with the shortest separation time, $\tau/T = 0.656$, where the second run-up is only slightly smaller than the first, case D with the lowest second run-up and $\tau/T = 1.185$, and case H where the two run-ups are nearly identical and $\tau/T = 1.892$. Figure 4.7(a)(b) shows the PIV results at two consecutive time frames in case A - right before and after the second wave enters the FOV. In this case the second wave arrives when the first wave is just about to start receding, as indicated by the near-zero velocity field right before the second wave arrives. Not surprisingly, the second run-up is not much lower than the first. On the other hand, Figure 4.7(c)(d) shows those for case D. Instead of a near-zero velocity field due to the first wave,

a receding flow can be seen retarding the second wave, causing a lowest second run-up. For case H, the second wave arrives after the first wave has completely receded from the FOV, leaving no water in the FOV. The observation in these three cases supports the claim that the second run-up is mainly determined by the flow field left by the first run-up.

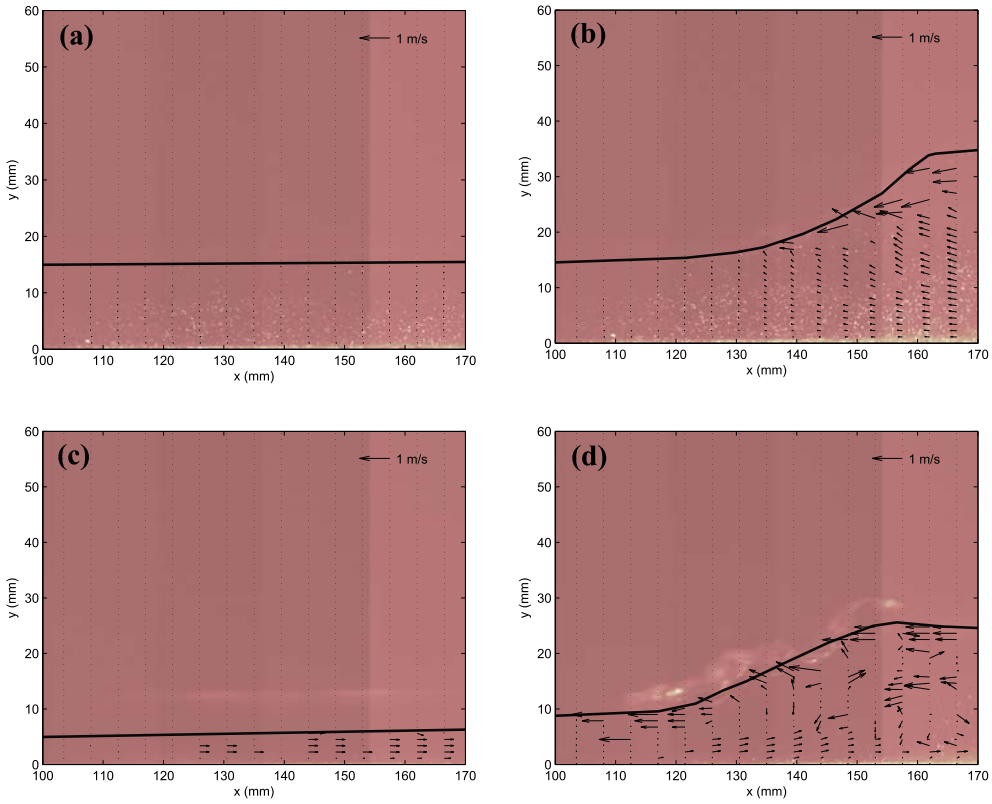

Figure 4.7: Snapshots of PIV results. *x* is the distance on the slope away from the still-water shoreline. The y-axis points upwards from the slope face. The wave travels towards the left. (a) Case A, right before the second wave arrives; (b) case A, right after the second wave arrives; (c) case D, right before the second wave arrives; (d) case D, right after the second wave arrives.

All PIV results will be compared in terms of depth-averaged mass and momentum fluxes at the center of the FOV. Ignoring the effects of air bubbles, we

can express the mass flux as ρUh, where U is the depth-averaged velocity in the direction parallel to the slope at the center of the FOV, h the local water depth, and ρ the density of water. The mass flux is then normalized by the mass influx of a solitary wave in the constant-depth region, ρcH; on the other hand, the momentum flux can be expressed as $\rho\overline{(u|u|)}h$, where $\overline{(u|u|)}$ is the depth-averaged sign-preserved velocity squared at the center of the FOV. The momentum flux is then normalized by $\rho c^2 H$; the results are shown in Figure 4.8. In case D where the lowest second run-up exists, the mass flux of the second wave is the lowest, suggesting less water volume being carried up the slope by the second wave because of the strongly receding first wave. As the separation time varies away from that in case D, the mass flux of the second wave increases, corresponding similarly to the spoon-shaped run-up trend. Although not as obvious, similar trend in momentum fluxes can be seen in Figure 4.8(c)(d). We remark here that the computation of momentum fluxes greatly amplifies experimental errors, since velocity squared is used. Thus, the small difference in momentum fluxes for cases D-H may not accurately represents the reality.

4.4 Reflected waves

With the run-up information known, the reflected waves on the $s = 1/2.47$ and $s = 1/20$ slopes are now examined further. *Park* [2009] first considered the reflection of two solitary waves from a $s = 1/20$ slope. It appears that for shorter separation times, only one reflected waves can be identified, whereas for longer separation times two reflected waves can be distinguished from one another. However, since the reflected waves from the slopes resemble dispersive and irregular long waves that change shapes significantly by the time they reach from

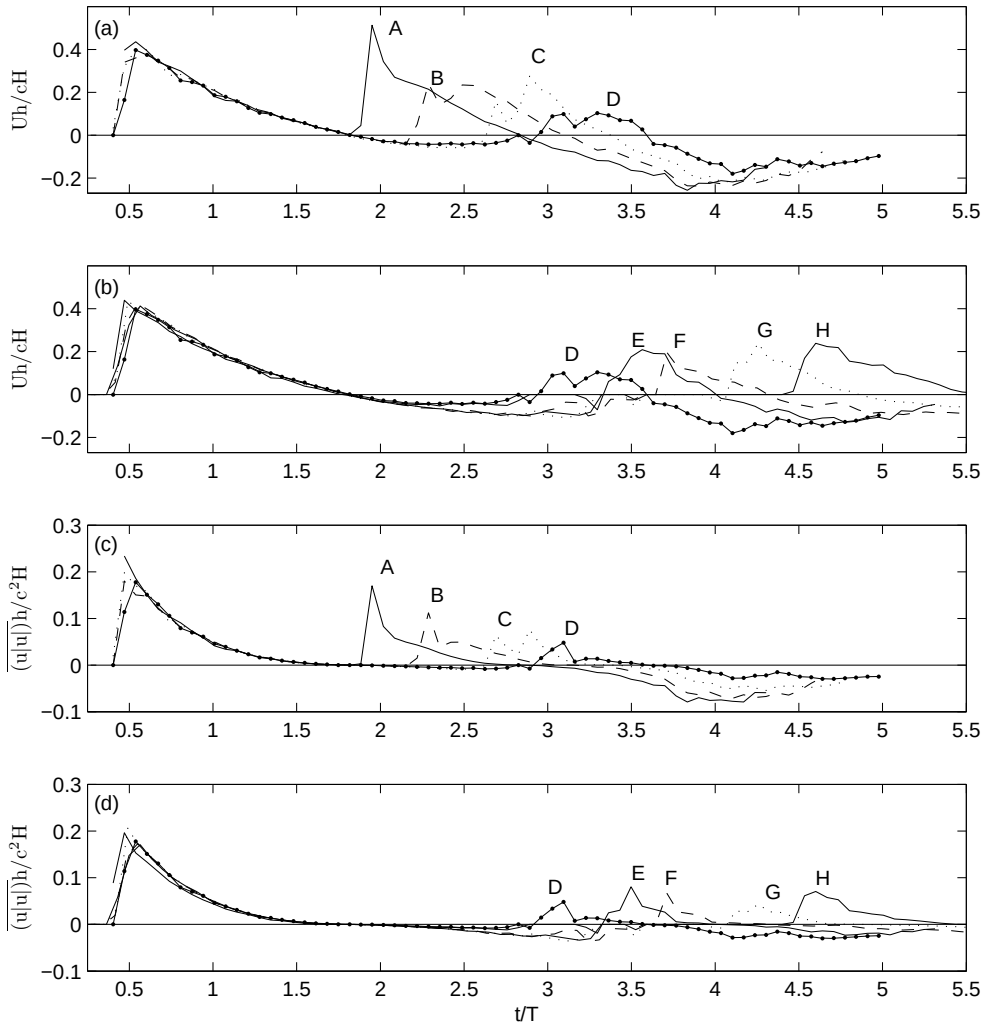

Figure 4.8: Normalized mass and momentum fluxes determined from PIV results. (a) Mass flux for cases A, B, C, and D; (b) mass flux for cases D, E, F, G, and H; (c) momentum flux for cases A, B, C, and D; (d) momentum flux for cases D, E, F, G, and H.

the slope the location of measurement, whether one can really distinguish one reflected wave from another remains questionable. To minimize the effect of dispersion, reflected waves measured right at the toe of the slope will be con-

sidered instead. A consistent way to compare the shapes of reflected waves is devised: a complete surface elevation measurement due to single solitary wave is treated as the surface elevation standard for solitary waves. When two waves exist with the separation time τ known, two surface elevation standards are linearly superposed with a time delay τ between the two, and the superposed result is then compared to the actual two-wave measurements. Such artificially superposed measurements have been found to be great indicators of the relation between reflected waves and the run-up trend. For each case on the $s = 1/20$ slope with $H/h = 0.15$, Figure 4.9 compares the two-wave measurements to the superposed ones, with the correlation coefficient r between the two calculated for each case. Interestingly, the correlation coefficients are higher, that is, the two resemble each other better, when the separation time is longer or shorter than the separation time that gives the lowest run-up, again showing a trend similar to the spoon-shaped run-up trend (based on Figure 4.6 the lowest second run-up occurs near $\tau/T = 1.233$). On the other hand, for the steep slope $s = 1/2.47$ where the spoon-shaped run-up trend doesn't show, the actual measurements and the superposed compare well for all cases, as shown in Figure 4.10 (note that on this slope the reflected wave at the toe of the slope cannot be separated from the incident wave). Based on the above observations, it can be suggested that in terms of surface elevation the wave-reflecting process can be approximated as linear, provided that the wave-wave interaction is minimal; namely, the two run-ups are not very different.

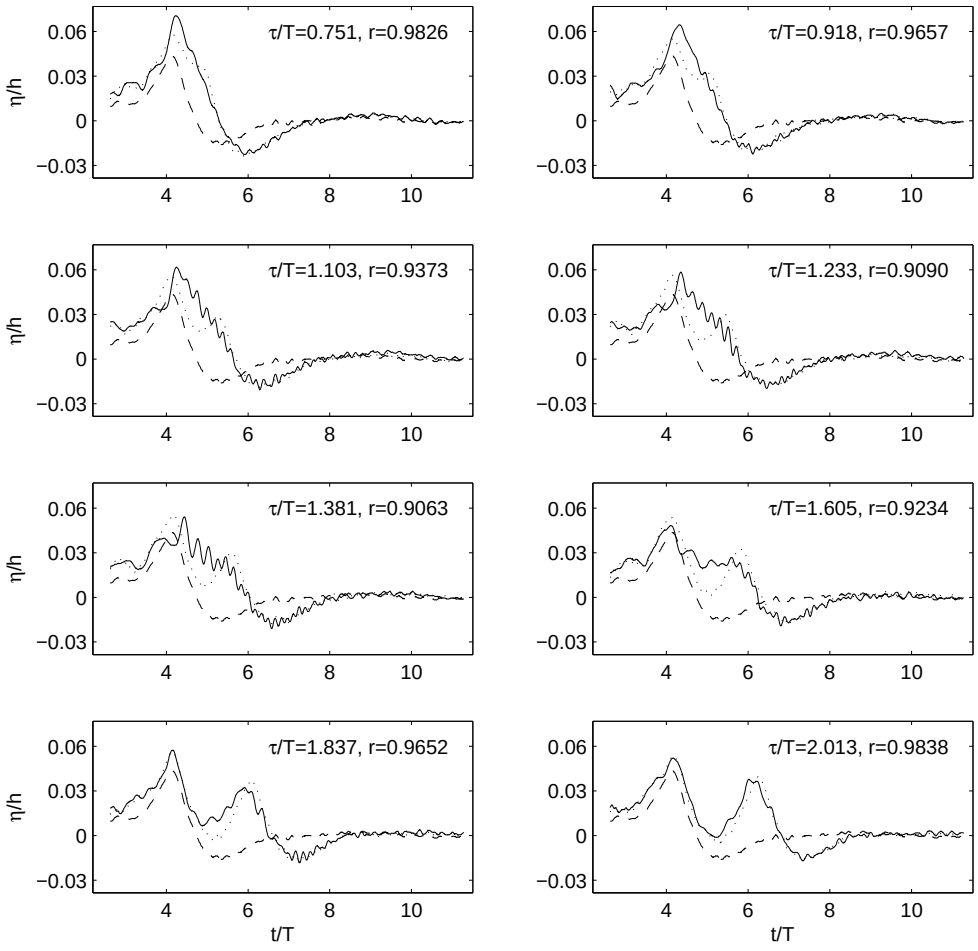

Figure 4.9: Reflections of double solitary waves from a $s = 1/20$ slope compared to superposed measurements, $H/h = 0.15$. $t/T = 0$ corresponds to the peak of the first incident wave. (—): two-wave measurement; (- - -): one-wave measurement; (···): superposed. r is the correlation coefficient between (—) and (···).

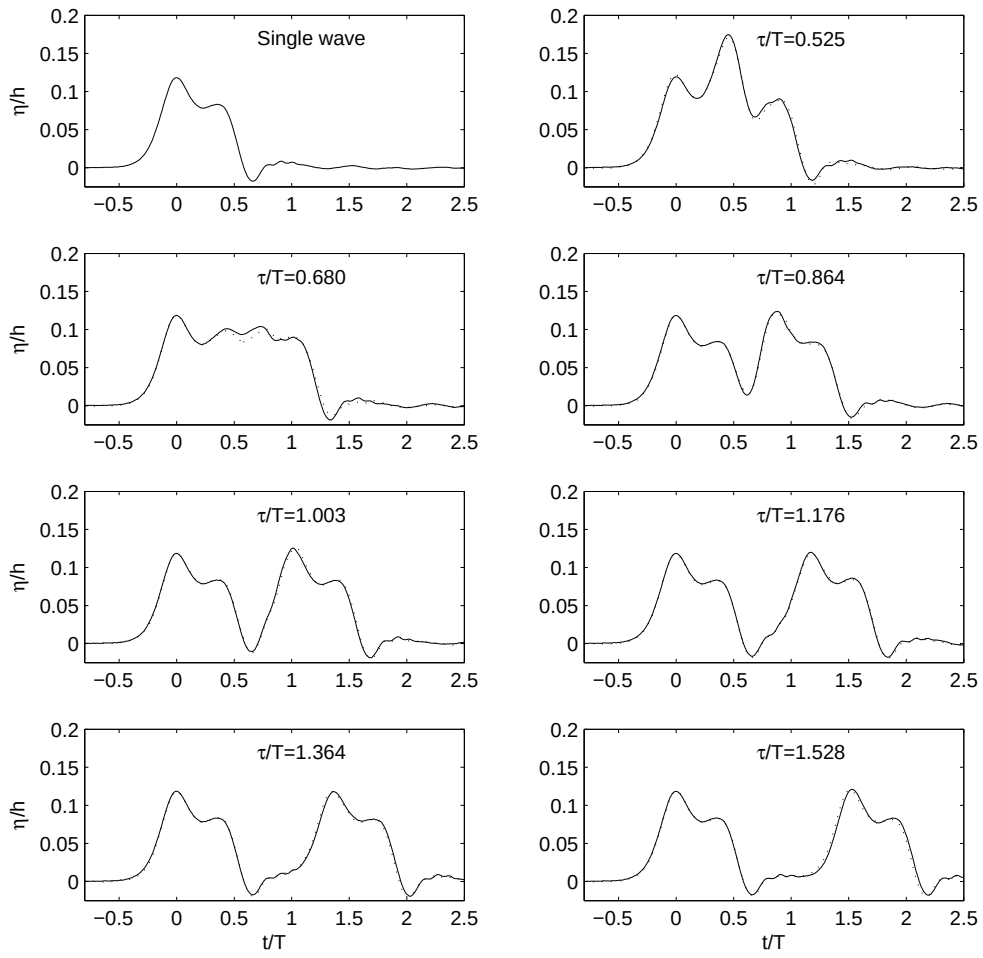

Figure 4.10: Reflections of double solitary waves from a $s = 1/2.47$ slope compared to superposed measurements, $H/h = 0.101$. $t/T = 0$ corresponds to the peak of the first incident wave. (—): two-wave measurement; (· · ·): superposed.

CHAPTER 5

CONCLUSION

Both single and double solitary waves were studied experimentally. The evolution and reflection of the waves were examined by monitoring the free surface elevations, the run-up heights measured by video cameras mounted on top of the slopes, and the two-wave interaction on the slope analyzed by employing PIV techniques. A theoretically-justified solitary wave surf parameter was proposed to characterize the run-up height of breaking solitary wave.

When plotting single solitary wave run-up in terms of fractional run-up, R/H, near the transition from non-breaking to breaking waves exists a maximum R/H value, which can be seen as the maximum fractional run-up on a given slope. It can be of value in engineering designs where a quick estimate of the maximum run-up is needed.

The run-up of double solitary waves was experimentally investigated and the physics explained. When two identical solitary waves are present, the first run-up heights remain more or less constant as the separation time between the two waves varies, whereas the second run-up heights show a “spoon-shaped” trend. When the separation time is long, the two run-up heights are identical; the second run-up decreases as the separation time shortens, until a lowest second run-up is reached. As the separation time shortens even more, the second run-up starts to increase instead; a second run-up higher than the first is found possible for very short separation time. An empirical equation was proposed to estimate the second wave run-up relative to the first.

The reflected waves from the slope correspond to the observed “spoon-shaped” run-up trend. When the two run-up heights are similar, the reflected two waves can be approximated by superposing two reflected single waves with specified separation time between the two, suggesting that in terms of free surface elevations the wave-reflecting process of two waves can be treated as linear if the two run-up heights are not very different.

BIBLIOGRAPHY

[1] Battjes, J. A. (1974), Surf similarity. Proc., 14th Coast. Engrg. Conf., ASCE, 1, 466–480.

[2] Briggs, M. J., Synolakis, C. E., Harkins, G. S. and Hughes, S. A. (1995), Large-scale, three dimensional laboratory measurements of tsunami inundation. *Tsunamis: Progress in Prediction, Disaster Prevention and Warning*, 129–149, Kluwer Academic Publishers, Netherlands.

[3] Carrier, G. F. and Greenspan, H. P. (1958), Water waves of finite amplitude on a sloping beach. *J. Fluid Mech.*, 17, 97–110, doi:10.1017/S0022112058000331.

[4] Chang, Y.-H., Hwang, K.-S. and Hwung, H.-H. (2009), Large-scale laboratory measurements of solitary wave inundation on a 1/20 slope. *Coastal Eng.*, 56, 1022–1034, doi:10.1016/j.coastaleng.2009.06.008.

[5] El, G. A., Grimshaw, R. H. J. and Tiong, W. K. (2012), Transformation of a shoaling undular bore. *J. Fluid Mech.*, 709, 371–395, doi:10.1017/jfm.2012.338.

[6] Fuhrman, D. R. and Madsen, P. A. (2008), Surf similarity and solitary wave run-up. *J. Waterway, Port, Coastal, Ocean Eng.*, 134, 195–198, doi:10.1061/(ASCE)0733-950X(2008)134:3(195).

[7] Galvin, C. J. (1968), Breaker type classification on three laboratory beaches. *J. Geophys. Res.*, 73, 3651–3659, doi:10.1029/JB073i012p03651.

[8] Gjevik, B. and Pedersen G. (1981), Run-up of Long Waves on an Inclined Plane. *Preprint Ser.* no. 2, Dept. of Maths, University of Oslo, Oslo, Norway.

[9] Goring, D. G. (1978), Tsunamis – The propagation of long waves onto a shelf. PhD thesis, California Institute of Technology, Pasadena, California.

[10] Grilli, S. T., Svendsen, I. A. and Subramanya, S. (1997), Breaking criterion and characteristics for solitary waves on slopes. *J. Waterway, Port, Coastal, Ocean Eng.*, 123, 102–112, doi:10.1061/(ASCE)0733-950X(1997)123:3(102).

[11] Grimshaw, R. (1971), The solitary wave in water of variable depth, Part 2. *J. Fluid Mech.*, 46, 611–622, doi:10.1017/S0022112071000739.

[12] Grue, J., Pelinovsky, E.N., Fructus, D., Talipova, T., and Kharif, C. (2008), Formation of undular bores and solitary waves in the Strait of Malacca caused by the 26 December 2004 Indian Ocean tsunami. *J. Geophys. Res.*, 113, C05008 doi:10.1029/2007JC004343, 2008.

[13] Hall, J. V. and Watts, J. W. (1953), Laboratory investigation of the vertical rise of solitary waves on impermeable slopes. *Tech. Memo.* 33, Beach Erosion Board, US Army Corps of Engineers.

[14] Hsiao, S.-C., Hsu, T.-W., Lin, T.-C. and Chang, Y.-H. (2008), On the evolution and run-up of breaking solitary waves on a mild sloping beach. *Coastal Eng.*, 55, 975–988, doi:10.1016/j.coastaleng.2008.03.002.

[15] Iribarren, C. R. and Nogales C. (1949), Protection des Ports II. Comm. 4, 17th Int. Navig. Congr., Lisbon, 31–80.

[16] Jensen, A., Pedersen, G. K. and Wood, D. J. (2003), An experimental study of wave run-up at a steep beach. *J. Fluid Mech.*, 461, 161–188, doi:10.1017/S0022112003004543.

[17] Kobayashi, N. and Karjadi, E. A. (1994), Surf-similarity parameter for breaking solitary wave run-up. *J. Waterway, Port, Coastal, Ocean Eng.*, 120, 645–650, doi:10.1061/(ASCE)0733-950X(1994)120:6(645).

[18] Langsholt, M. (1981), Experimental study of wave run-up. Cand.real. thesis, University of Oslo, Oslo, Norway.

[19] Li, Y. and Raichlen, F. (2001), Solitary wave runup on plane slopes. *J. Waterway, Port, Coastal, Ocean Eng.*, 127, 33–44, doi:10.1061/(ASCE)0733-950X(2001)127:1(33).

[20] Li, Y. and Raichlen, F. (2002), Non-breaking and breaking solitary wave run-up. *J. Fluid Mech.*, 456, 295–318, doi:10.1017/S0022112001007625.

[21] Madsen, P. A., Fuhrman, D. R. and Schäffer, H. A. (2008), On the solitary wave paradigm for tsunamis. *J. Geophys. Res.*, 113, C12012, doi:10.1029/2008JC004932.

[22] Mei, C. C. (1989), *The Applied Dynamics of Ocean Surface Waves, Advanced Series on Ocean Engineering*, vol. 1, World Scientific, Singapore.

[23] Park, Y. S. (2009), Seabed dynamics and breaking waves. PhD thesis, Cornell University, Ithaca, New York.

[24] Peregrine, D. H. (1966), Calculations of the development of an undular bore. *J. Fluid Mech.*, 25, 321–330, doi:10.1017/S0022112066001678.

[25] Synolakis, C. E. (1987), The runup of solitary waves. *J. Fluid Mech.*, 185, 523–545, doi:10.1017/S002211208700329X.

[26] Zelt, J. A (1991), The run-up of non-breaking and breaking solitary waves. *Coastal Eng.*, 15, 205–246, doi:10.1016/0378-3839(91)90003-Y.